Discretized Clay Shell Model (DCSM) of Clayey Sandstone: Evaluating the Effective Stress Coefficient of Permeability

P. L. Tai[1], and J. J. Dong[1, 2]

[1]Graduate Institute of Applied Geology, National Central University, Taoyuan 32001, Taiwan

[2]Earthquake-Disaster & Risk Evaluation and Management Center, National Central University, Taoyuan 32001, Taiwan

Corresponding author: Jia-Jyun Dong (jjdong@geo.ncu.edu.tw)

Key Points:

- We propose Discretized Clay Shell Model (DCSM) to account for the stress dependent shear modulus of clay domain.
- DCSM predicts a pore pressure and confining stress dependent effective stress coefficient of clayey sandstones.
- The predicted α are generally different from 1 and assuming $\alpha = 1$ could be problematic for estimating permeability.

Abstract

The effective stress coefficient α determines the effective stress, which dominating the permeability of rocks. However, the documented value of α for rocks shows a high scatter (0.3-5.5), based on the laboratory measurement. The well know Clay Shell Model (CSM) successfully explain why the α of the clayey sandstone can well above 1 theoretically. However, CSM cannot account

for the stress dependency of α observed experimentally. In this study, a modification of CSM was proposed. This proposed Discretized Clay Shell Model (DCSM) discretizes multi-layers clay domain to account for the stress dependent elastic modulus of clay and calculates the pore radius of DCSM model under different confining stress σ_c and pore pressure P_p. Iso-pore radius curves under different σ_c and P_p was used to determine the α. The parametric study illustrates the superior features of the proposed DCSM to the traditional CSM. Critical findings include: (1) The predicted α form a concaving upward surface in the pore pressure-confining stress space using DCSM. (2) The influence of P_p on α will be stronger than the influence of σ_c especially under low P_p. (3) The predicted α is not necessary positively or negatively correlated to σ_c under constant P_p. (4) The predicted α for soft, high stress dependent deformability of clay coating on the pores of sandstones could be far higher than 1. Two synthetic cases (laboratory and in-situ scale) illustrate the importance of stress dependent (σ_c and P_p) effective stress coefficient α for determining the effective stress and permeability.

1 Introduction

The stress dependent permeability k of sandstone, one of the important reservoirs, is a key parameter for fossil fuel exploitation (e.g., Li et al., 2008) and carbon geological sequestration (e.g., Cui et al., 2007). The general stress dependency of permeability k can be expressed as $k = f(\sigma_c, P_p)$, where σ_c is confining stress and P_p is pore pressure. This two-variable function can be replaced by a single variable function $k = f(\sigma_{eff})$ if an effective stress principle is valid (e.g.,

Bernabe, 1987; Al-Wardy and Zimmerman, 2004; Li et al., 2009; 2014), where σ_{eff} is the effective confining stress (briefly "effective stress" thereafter).

The effective stress dominating the permeability of rocks has been defined by many researchers (e.g., Bernabe, 1987; Berryman, 1992; Al-Wardy and Zimmerman, 2004; Li et al, 2009, 2014) as follows:

$$\sigma_{eff} = \sigma_c - \alpha P_p \tag{1}$$

where α is effective stress coefficient for permeability. This parameter α is a measure of the relative sensitivity of pore pressure and confining pressure to the permeability k (Al-Wardy and Zimmerman, 2004). If α is a constant, the effective stress σ_{eff} can be determined by σ_c and P_p, experimentally (e.g., Zoback and Byerlee, 1975; Walls and Nur, 1979; Al-Wardy and Zimmerman, 2004; Ghabezloo et al., 2009). Traditionally, the effective stress principle proposed by Terzaghi (1943) assumed $\alpha = 1$.

When the confining stress are significantly larger than the pore pressure (e.g., permeability measurement in laboratory under high confining stress), precise determination of the effective stress coefficient α may not be critical due to minor contribution of the P_p to effective stress when Eq. (1) was used. However, many sedimentary basins on continental margins hold hydrostatic or abnormally high pore pressure at depths (Breckels, 1982; Gaarenstroom et al., 1993; Engelder and Fischer, 1994). The parameter α become critical for predicting the permeability k at burial depth. Moreover, the de-pressurization during the production lifecycle of a reservoir changes the pore pressure P_p and the effective stress σ_{eff} can only be evaluated when α can be determined in prior. Although effective stress dependent relations of permeability are available (e.g., Dong et al., 2010), the prediction of permeability-depth relation are still challenge for the effective stress coefficient α at different burial depth subjected to a high variety of stress combinations cannot be determined confidently.

For most of the rocks (e.g., crystalline rocks, clean granular rocks, chalks, shales and so forth), the values of α close to but lower than 1 have been reported (e.g., Berryman, 1992). Some experimental studies found α of clayey sandstone and tight sandstone range in 0.60 to 0.85. (e.g. Abass et al., 2009). However, Zoback and Byerlee (1975) measured permeability of the clayey Berea sandstone and found the α is ranging from 2.20 to 4.00. This result was supported by other experimental studies such as Walls and Nur (1979). To account for the observations of α larger than 1, Zoback and Byerlee (1975) proposed a conceptual model, Clay Shell Model (CSM). They suggested soft clay coating on wall of grains (e.g., double layers) and the shape of pores is assumed as cylinder. The grains, clay and pores system of clayey sandstones was conceptualized in Fig. 1(a).

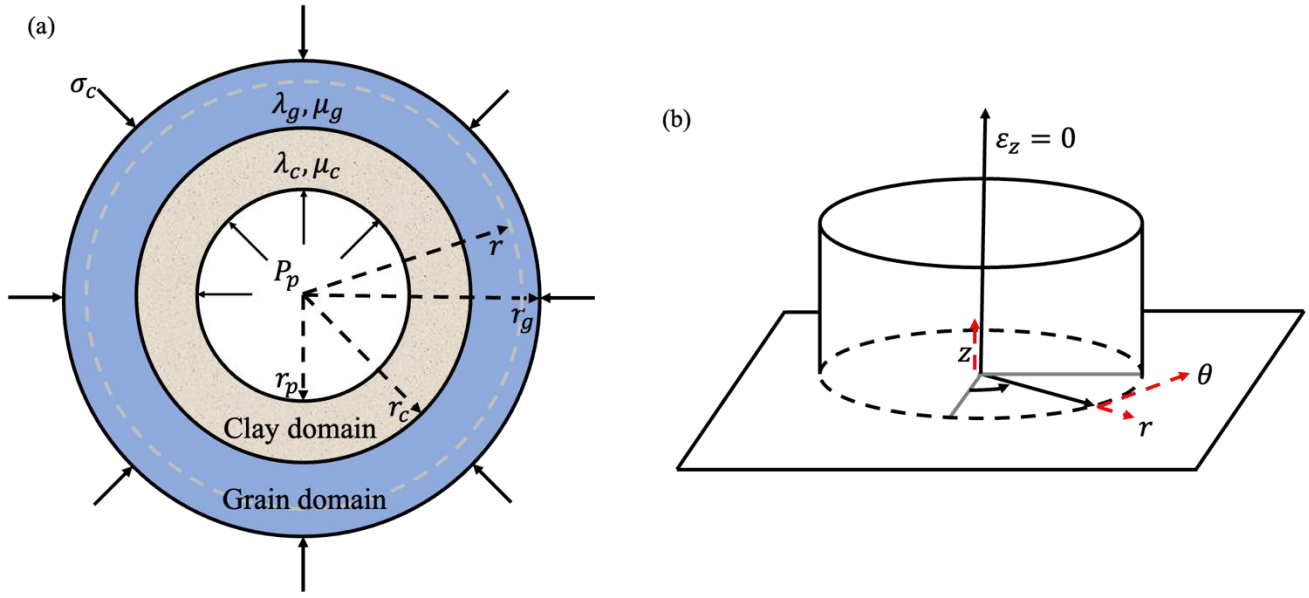

Figure 1. (**a**) Clay Shell Model (CSM, modified from Al-Wardy and Zimmerman, 2004) for clayey sandstone. The clayey sandstone was conceptualized as grains, clay, and pore system; (**b**) Cylinder pore and the plane strain condition (vertical strain (in direction of z axis) equals to zero). The cylindrical polar coordinate was selected.

In Fig. 1(a), the r is the radial distance from the center of pore to a specific point within the clay and grain domains. The r_p, r_c and r_g are the pore radius, distance from the center to the inner and outer boundaries of grains, respectively. The domain between r_p and r_c is composed of clay, and the domain between r_c and r_g is composed of sand grains. The μ_g and μ_c are the shear modulus of grain (between r_c and r_g) and clay (between r_p and r_c), respectively. The λ_g and λ_c are the Lamé constant of grain (between r_c and r_g) and clay (between r_p and r_c), respectively. The variation of r_p versus σ_c and P_p determines the effective stress coefficient for deformability and porosity $\phi(=\frac{r_p^2}{r_g^2})$, as well as for the permeability, which will be introduced in more detail later (Section 2.1).

Since the elastic moduli of the clay are usually smaller than the moduli of grains, the influence of pore pressure on the pore radius should be larger than the influence of confining pressure. That is, this heterogeneity of clayey sandstones resulted in $\alpha > 1$ (Zoback and Byerlee, 1975). Al-Wardy and Zimmerman (2004) elaborated the CSM further following the idea proposed by Zoback and Byerlee (1975). Based on CSM (details will be introduced in Section 2.2), the effective stress coefficient α will be function of shear modulus of grains and clay, as well as the clay fraction F_c defined as follows:

$$F_c = \frac{r_c^2 - r_p^2}{r_g^2 - r_p^2} \tag{2}$$

The derived α from CSM is a constant which is irrelevant to the variation of confining stress σ_c and pore pressure P_p, which is contradict to the observations of many previous studies (Todd and Simmons, 1972; Coyner, 1984; Gangi and Carlson, 1996). Notably, the elastic moduli of clay and grains are assumed as stress independent for the CSM. It is not a realistic assumption ,since the elastic moduli of clay are stress-dependent. According to the wave velocity and density measurement (Mondol et al., 2008), the shear moduli of clay can elevated from 0.88 GPa to 2.74 GPa when the confining stress increased from 5 MPa to 50 MPa. Since the α should not be a constant but varied

with changing σ_c and P_p, the equation used to calculate the effective stress would be modified slightly from Eq. (1) (e.g. Robin, 1973; Li et al., 2009; 2014) to Eq. (3):

$$\sigma_{eff} = \sigma_c - \alpha_{(P_p,\sigma_c)} \cdot P_p \tag{3}$$

The $\alpha_{(P_p,\sigma_c)}$ is a pore pressure/confining stress dependent (named as "stress dependent" thereafter) effective stress coefficient.

In this study, the stress dependency of elastic moduli of clay will be incorporated into the CSM to depict the complicate relationship between α, σ_c and P_p. We discretized the clay domain into several thin rings to calculate the stress dependent elastic moduli of clay at different radial distance r to the center of pore. Using this proposed Discretized Clay Shell Model (DCSM) to calculate the r_p under different σ_c and P_p. The variation of α with pore pressure P_p and confining stress σ_c can be determined without difficulties by iso-pore radius curves. The experimental data of stress dependent elastic moduli of kaolinite power (Unconsolidation) documented by Mondol et al. (2008), as well as two more synthetic clay with different stress sensitive of elastic moduli, were incorporated into the DCSM to evaluate the influence of pore pressure P_p and confining stress σ_c, together with clay fraction F_c, porosity ϕ, and stress dependent elastic modulus of clay on $\alpha_{(P_p,\sigma_c)}$.

Moreover, previous measurement results of α for clayey sandstones is controversial. We provide possible explanations based on the calculation results of proposed DCSM. Finally, two synthetic cases (laboratory and in-situ scale), which the range of pore pressure P_p and confining stress σ_c are quite different, were provided. The stress dependent effective stress coefficient $\alpha_{(P_p,\sigma_c)}$ was determined using the proposed DCSM. The effective stress, as well as the permeability, can thus been calculated. The importance of relation between pore pressure P_p, confining stress σ_c, and stress dependent effective stress coefficient α to the determination of effective stress and permeability will be illustrated accordingly.

2 Clay Shell Model (CSM) and stress independent effective stress coefficient α

2.1 Stress independent effective stress coefficient α of permeability

If the effective stress coefficient α is stress independent (independent of confining stress σ_c and pore pressure P_p), Eq. (1) can be used to predict the effective stress. Under this assumption, Bernabe (1987) proposed Eq. (4) to calculate the effective stress coefficient α for permeability via the permeability measurement under different pore pressure P_p and confining stress σ_c:

$$\alpha = -\frac{\left(\frac{\partial k}{\partial P_p}\right)_{\sigma_c}}{\left(\frac{\partial k}{\partial \sigma_c}\right)_{P_p}} \tag{4}$$

where $\left(\frac{\partial k}{\partial P_p}\right)_{\sigma_c}$ and $\left(\frac{\partial k}{\partial \sigma_c}\right)_{P_p}$ are partial derivative of permeability k to pore pressure P_p and confining stress σ_c, respectively. Based on the Hagen-Poiseuille equation and Darcy's law, the permeability k along a cylindrical tube can be expressed as (e.g. Civan et al., 2011; Cao et al., 2016):

$$k = \frac{r_p^4}{8r_g^2} \tag{5}$$

where the r_p and r_g are the radius of pore and grain (Fig. 1(a)), respectively. If the r_g assumed as constant (Eulerian permeability) and insert Eq. (5) into Eq. (4), the effective stress coefficient α can be calculated using following equation:

$$\alpha = -\frac{\left(\frac{\partial r_p}{\partial P_p}\right)_{\sigma_c}}{\left(\frac{\partial r_p}{\partial \sigma_c}\right)_{P_p}} \tag{6}$$

That is, the effective stress coefficient α for permeability can be determined based on the pore radius variations. The theory background of CSM (variations of r_p with σ_c and P_p) will be introduced in the following section.

2.2 Clay Shell Model (CSM) for Clayey sandstones

CSM conceptualized the clayey sandstones into a system with hollow cylinder pore in grains coating by clay (Fig. 1(a)). If the variations of r_p with σ_c and P_p can be evaluated, the α can be obtained using Eq. (6). Based on plain strain assumption (Fig. 1(b)) and axial symmetry, the calculation is simply 1-D problem. The only component relevant to r_p is the radial displacement vector $u_{(r)}$ along radius of cylindrical polar coordinate (Fig. 1(b)). The derivation of the relationship between $u_{(r)}$ and stress condition (σ_c and P_p) can be found in textbook of elastic theory (e.g., Sokolnikoff, 1956; Jaeger and Cook, 1979). The basic idea was introduced briefly here to better illustrate our proposed model in Section 3.1.

For a hollow, homogeneous tube, the radial displacement $u_{(r)}$ at radial location r from the center of the tube to a specific point can be expressed as:

$$u_{(r)} = Ar + \frac{B}{r} \tag{7}$$

The A and B are parameters related to elastic moduli of the material composed of the tube. To solve A and B, the relation between radial stress σ_r and radial displacement $u_{(r)}$ is required as follows (Sokolnikoff, 1956):

$$(\lambda + 2\mu)\frac{du_{(r)}}{dr} + \lambda\frac{u_{(r)}}{r} = \sigma_r \tag{8}$$

where λ and μ are Lamé constant and shear modulus. Two boundary conditions are used: the radial stress σ_r at $r = r_p$ is P_p and σ_r at $r = r_g$ is σ_c. Therefore,

$$(\lambda + 2\mu)(A - \frac{B}{r_p^2}) + \lambda(A + \frac{B}{r_p^2}) = P_p \tag{9a}$$

$$(\lambda + 2\mu)(A - \frac{B}{r_g^2}) + \lambda(A + \frac{B}{r_g^2}) = \sigma_c \tag{9b}$$

The two unknowns A and B can be solved via these two boundary conditions (Eqs. (9a) and (9b)). The radial displacement when $r = r_p$ can be expressed by Eq. (10):

$$u_p = Ar_p + \frac{B}{r_p}, \tag{10}$$

where u_p denotes the displacement of pore radius. The u_p can be used to calculate the variation of pore radius r_p caused by σ_c and P_p, and the effective stress coefficient α can be determined using Eq. (6).

For CSM, the hollow tube model includes two materials (clay and grain domains in Fig. 1(a)). The parameters A and B for clay and grain domains will be different. We use the A_c and B_c representing the parameters for clay domain and A_g and B_g for grain domain (totally four unknowns). The Lamé constant λ_c and λ_g, and the shear modulus μ_c and μ_g were elastic moduli for clay and grain domains, respectively. Notably, the elastic moduli of clay and grain were assumed as stress independent in CSM.

Two boundary conditions, Eqs. (11a) and (11b), are not enough to solve the four unknowns. However, we have two compatibility conditions of radial stress (Eq. (11c)) and displacement (Eq. (11d)) which must be satisfied when $r = r_c$ (see Fig. 1(a)).

$$(\lambda_c + 2\mu_c)(A_c - \frac{B_c}{r_p^2}) + \lambda_c(A_c + \frac{B_c}{r_p^2}) = P_p \tag{11a}$$

$$\left(\lambda_g + 2\mu_g\right)(A_g - \frac{B_g}{r_g^2}) + \lambda_g(A_g + \frac{B_g}{r_g^2}) = \sigma_c \tag{11b}$$

$$(\lambda_c + 2\mu_c)\left(A_c - \frac{B_c}{r_c^2}\right) + \lambda_c\left(A_c + \frac{B_c}{r_c^2}\right) = \left(\lambda_g + 2\mu_g\right)(A_g - \frac{B_g}{r_c^2}) + \lambda_g(A_g + \frac{B_g}{r_c^2}) \tag{11c}$$

$$A_c r_c + \frac{B_c}{r_c} = A_g r_c + \frac{B_g}{r_c} \tag{11d}$$

Based on two boundary conditions (Eq. (11a) and Eq. (11b)) and two compatibility conditions at $r = r_c$ ((Eq. (11c) and Eq. (11d))), the four unknowns (A_c and B_c; A_g and B_g) can be solved and the displacement of pore radius can be calculated via Eq. (12) accordingly.

$$u_p = A_c r_p + \frac{B_c}{r_p} \tag{12}$$

Eq. (12) can be substituted into Eq. (6) to evaluate the effective stress coefficient α. Although the variation of pore radius were influenced by stress condition (σ_c and P_p), the α is stress-independent in CSM. The α was only influence by clay fraction F_c, porosity ϕ, Poisson's ratio ν, and shear modulus ratio γ (defined in Eq. (13)), which can be found in Al-Wardy and Zimmerman (2004).

$$\gamma = \frac{\mu_g}{\mu_c} \tag{13}$$

Figure 2 shows the predicted α of sandstones with clay fraction F_c from 0 to 0.3 using CSM (Al-Wardy and Zimmerman, 2004). Five curves represent the different α when γ (ratio of shear modulus between grains and clay) equal to 1, 5, 10, 25, 50. The porosity ϕ of the clayey sandstones equals to 0.2. The Poisson's ratio ν of clay and grains equals to 0.25. It should be note that the pore volume within the clay is neglected in Al-Wardy and Zimmerman (2004) for calculating the clay fraction and porosity. This study adopted this assumption as well.

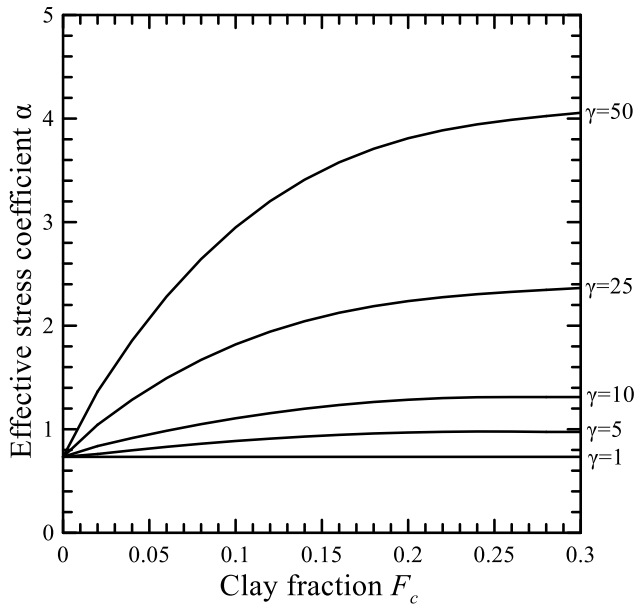

Figure 2. The predicted α of clayey sandstones using CSM with porosity $\phi = 0.2$, under different clay fraction F_c and shear modulus ratio γ. The Poisson's ratio $\nu = 0.25$ for grains and clay.

(modified from Al-Wardy and Zimmerman, 2004)

When $\gamma = 1$ or $F_c = 0$, which represent a clean sandstone, the $\alpha = 0.713$. This value can be obtained analytically (Al-Wardy and Zimmerman, 2004). Generally, the effective stress coefficient α increases with increasing γ (decreases the shear modulus of clay while the shear modulus of grains is remains unchanged) and clay fraction F_c.

Since the elastic moduli of clay and grains are assumed as stress-independent in CSM, the determined effective stress coefficient α is a constant when the F_c and γ are fixed and will not vary with changing confining stress σ_c and pore pressure P_p. As aforementioned, the shear modulus of clay when confining stress equals to 50 MPa can be three times of the one under confining stress equals to 5 MPa (Mondol et al., 2008). It is not realistic to assume the elastic moduli of clay as stress-independent. The elastic moduli of clay at different r should be different since the radial stress σ_r is not a constant, which will be illustrated in Section 3.1. Moreover, Eq. (6) used by Al-Wardy and Zimmerman (2004) for determining the α of CSM is no more valid if α is stress dependent. This study adopted the approach used by (Warpinski and Teufel, 1992; Li et al., 2009; 2014) to determine α, which will be introduced in Section 3.2.

3 Discretized Clay Shell Model (DCSM) and stress dependent effective stress coefficient $\boldsymbol{\alpha_{(\sigma_c, P_p)}}$

To account for the elastic moduli heterogeneity of clay due to radial stress heterogeneity (stress-dependent elastic moduli), this study proposed a Discretized Clay Shell Model (DCSM), which is a modification of traditional Clay Shell Model (CSM). We introduced the DCSM first (Section 3.1) and the derivation of stress dependent effective stress coefficient $\alpha_{(\sigma_c, P_p)}$ subsequently (Section 3.2).

3.1 Discretized Clay Shell Model (DCSM)

This study discretized clay domain in Fig. 1(a) into numerous thin rings to account for the stress dependent elastic moduli of clay. There are two tasks to be solved: (1) the number of material parameters (A and B in CSM) involved to be solved increasing with increased rings; (2) the radial stress at different ring is required for calculating the elastic moduli of clay.

Figure 3 shows the concept of Discretized Clay Shell Model (DCSM). The r_p is the pore radius. The r_i (i=0~N, $r_0 = r_p$) represents the outer radius of i-th ring. Here, the r_N ($i = \mathrm{N}$) is equivalent to the outer boundary of clay domain r_c defined in previous sections. The Poisson's ratio and shear modulus of i-th ring denoted by ν_i and μ_i. It should be mentioned here that the elastic moduli of material were Lamé constant and shear modulus in Fig. 1(a). The Poisson's ratio will replace the Lamé constant subsequently. The ν_i and μ_i of clay domain are the functions of radial stress σ_r and location r, which will be introduced in Section 4.2.

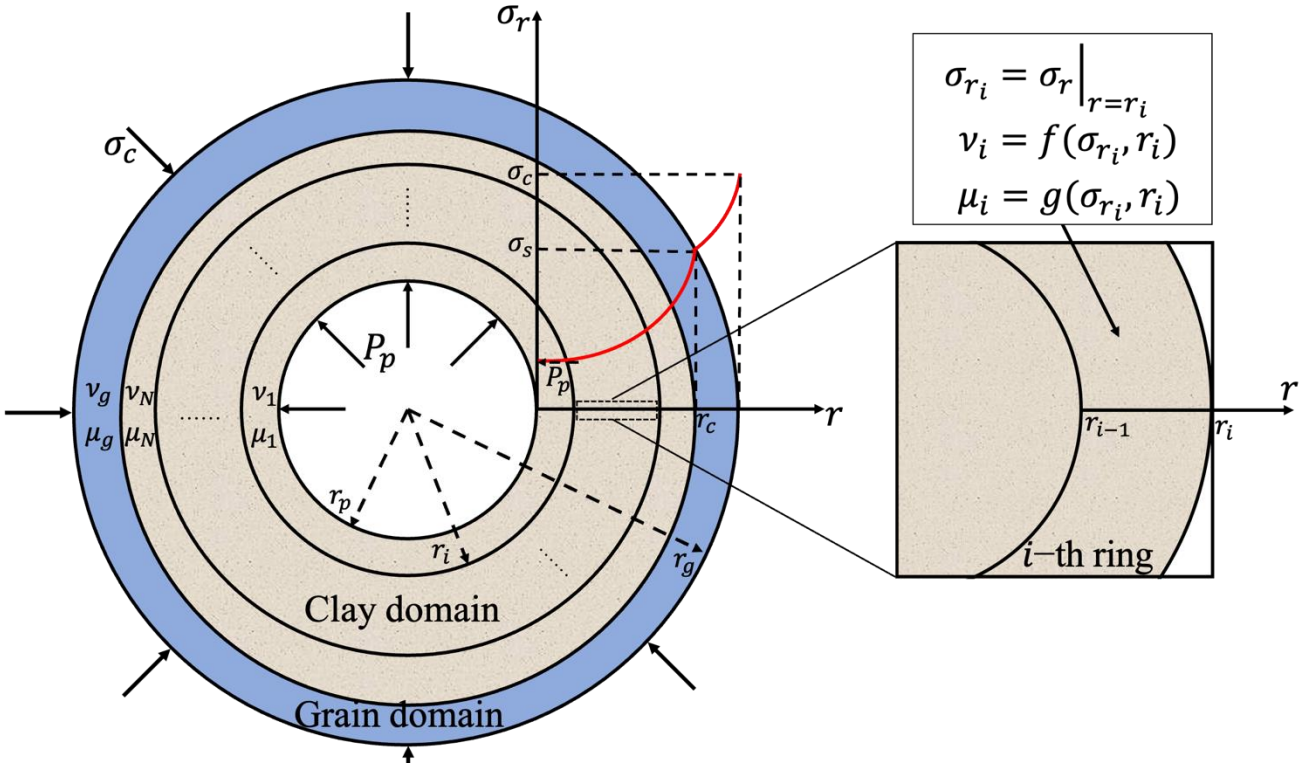

Figure 3. The Discretized Clay Shell Model (DCSM). There are N rings with different elastic moduli ν_i and μ_i in clay domain. The r_p is the pore radius. The r_i is the outer boundary of the *i*-th ring. For the stress dependency of grain elastic moduli is insignificant, one ring for grain domain could be enough for the moduli are relatively homogeneous.

The parameters of A and B in Eq. (7) for each ring are different and can be denoted by A_j and B_j ($j = 1{\sim}\mathrm{N}+1$, 1~N belong to clay domain, and number N+1 denotes grain domain). Therefore, totally 2(N+1) unknowns need to be solved (There are N layers in clay domain, and single layer in grain domain for the moduli of grain is relatively homogeneous). As aforementioned (Section 2.2), there are 4 unknowns (A_c and B_c; A_g and B_g) were solved for CSM via 2 boundary conditions (pore pressure and confining pressure applied on the inner boundary of clay domain and outer boundary of grain domain) and 2 compatibility conditions (radial stress and displacement are identical on the boundary of clay and grains domains). Likewise, there are two boundary conditions

and 2N compatibility conditions (radial stress and displacement on boundary of *i*-th ring and the (*i*+1)-th ring) in DCSM. Totally 2(N+1) equations were available to solve the 2(N+1) unknowns (A_j and B_j, $j = 1 \sim \mathrm{N} + 1$).

In this study, the stress dependent elastic moduli can be characterized. Details can be found in Section 4.2. We assumed the values of elastic moduli (ν_i and μ_i) of clay in all layers (Fig. 3) are identical (the ones when $\sigma_r = 0$ MPa) first. A_j and B_j can thus be determined by aforementioned steps. Then, we calculate the radial stress σ_r of each layer using Eq. (14):

$$(\lambda_i + 2\mu_i)(A_i - \frac{B_i}{r_i^2}) + \lambda_i(A_i + \frac{B_i}{r_i^2}) = \sigma_{r_i} \tag{14}$$

The determined radial stress of each layer via Eq. (14) can be used to determine the new elastic moduli ν_i and μ_i of each layer, using the stress dependent elastic moduli characterized in Section 4.2. The new elastic moduli produce new A_j and B_j of each layer and new radial stress will obtain. This process will be iterative until the absolute relative error less than 10^{-3}. The displacement of pore radius (u_p) can thus be determined by Eq. (15) with the determined parameters (A_1 and B_1) for the 1st ring:

$$u_p = A_1 r_p + \frac{B_1}{r_p} \tag{15}$$

The displacement of pore radius u_p under different σ_c and P_p in DCSM can be used to determine the effective stress coefficient $\alpha_{(P_p,\sigma_c)}$, if the iso-pore radius under different confining stress and pore pressure can be obtained (explained in Section 3.2). The effective stress coefficient $\alpha_{(P_p,\sigma_c)}$ is function of σ_c and P_p and will not be a constant anymore.

3.2 Using iso-pore radius curves to determine the stress dependent effective stress coefficient $\alpha_{(P_p,\sigma_c)}$

The response surface method proposed by Box and Draper (1987) was used by Warpinski and Teufel (1992) and Li et al. (2009; 2014) to determine the effective stress coefficient $\alpha_{(\sigma_c,P_p)}$. The original response surface uses the relation between permeability ($k_{(P_p,\sigma_c)}$), confining stress σ_c and pore pressure P_p. Based the effective stress principle, the iso-permeability under different σ_c and P_p will therefore be the iso-effective stress and $\alpha_{(\sigma_c,P_p)}$ can be determined. Based on Eq. (5), we can use the variations of the pore radius r_p (can be calculated by displacement of pore radius u_p determined by the proposed DCSM) due to changing of σ_c and P_p to represent the stress dependent permeability $k_{(P_p,\sigma_c)}$. The relation of pore radius r_p to the confining stress σ_c and pore pressure P_p can be depicted as a surface and illustrated in Fig. 4(a). Figure 4(b) is a horizontal projection of Fig. 4(a). The contours in Fig. 4(b) are iso-r_p curves where the pore radius under different confining stress and pore pressure are identical. That is, the iso-r_p curves in Fig. 4(b) are iso-*k* curves, too. As aforementioned, if the effective stress principle is valid, the iso-*k* curve can also be the iso-σ_{eff} curves.

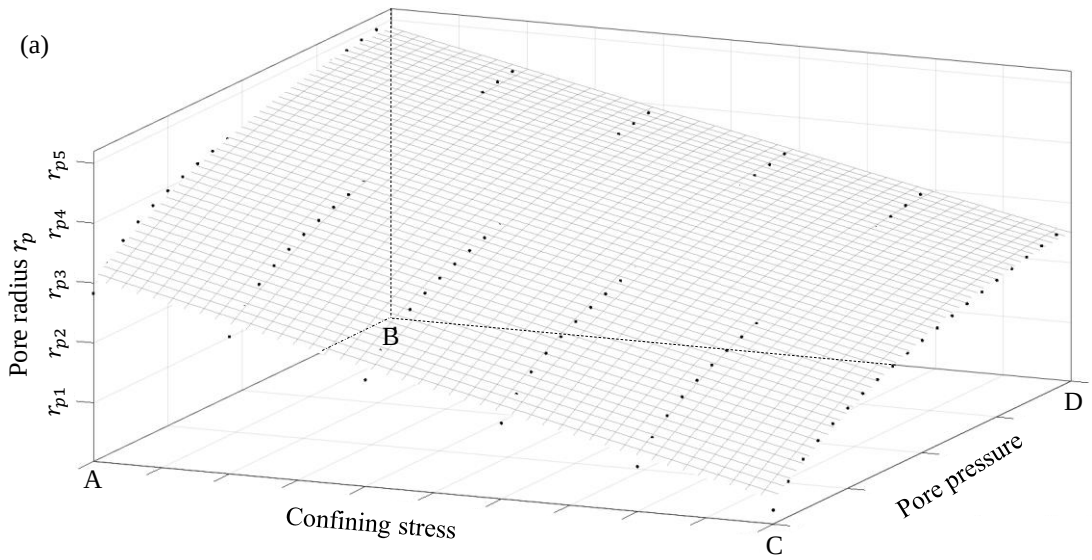

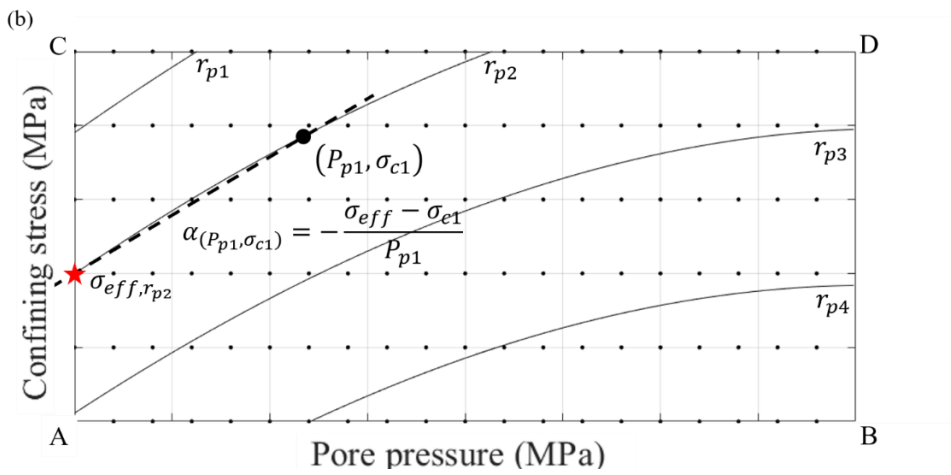

Figure 4. Using iso-pore radius curves for determining the effective stress coefficient $\alpha_{(\sigma_c,P_p)}$. (**a**) Variations of pore radius versus changing of confining stress and pore pressure; (**b**) The contours of pore radius under different confining stress and pore pressure, each curve represents iso-r_p curve. The $\alpha_{(\sigma_c,P_p)}$ will be the secant slope between red star and black circle, according to the approach used by Warpinski and Teufel (1992) and Li et al. (2009; 2014).

If the effectives stress coefficient α is a constant (independent of σ_c and P_p), the surface in Fig. 4(a) should be a plane. The iso-r_p curves in Fig. 4(b) will be straight lines. According to Eq. (1), the effective stress will equal to confining stress when $P_p = 0$. That is, the intercepts of the iso-r_p curves and the confining stress axis are effective stress, such as the star marked on Fig. 4(b). The slope of iso-r_p lines actually are effective stress coefficient α according to Eq. (1). The α would also be the same by using Eq. (6) if the surface in Fig. 4(a) is a plane.

If the effectives stress coefficient α is stress dependent, the slopes of iso-r_p (when $r_p = r_{p2}$) curves in Fig. 4(b) will vary with pore pressure and confining stress. According to Eq. (3), the effective stress coefficient $\alpha_{(P_{p1},\sigma_{c1})}$ (when the confining stress and the pore pressure equal to σ_{c1} and P_{p1}, circle on Fig. 4(b)) can be determined as:

$$\alpha_{(P_{p1},\sigma_{c1})} = -\frac{\sigma_{eff}-\sigma_{c1}}{P_{p1}}, \tag{16}$$

since the iso-r_p curves represent the iso-σ_{eff} curves and the y-axis of stars in Fig. 4(b) represents the σ_{eff} when $r_p = r_{p2}$. That is, the stress dependent effectives stress coefficient $\alpha_{(P_p,\sigma_c)}$ is the secant slope of dashed line connecting star (0, $\sigma_{eff,r_{p2}}$) and circle (P_{p1}, σ_{c1}) marked on Fig. 4(b).

4 Geometry and material properties used in DCSM

4.1 Geometry and boundary conditions (confining stress and pore pressure)

The initial outer boundary of grain domain r_g=25.82 μm and inner boundary of clay domain (pore radius) r_p=10.00μm to make the porosity ϕ equals to 0.2 which is identical to the ones selected by Al-Wardy and Zimmerman (2004) for CSM. The clay domain were divided into 10^4 rings, for evaluating the radial stress and elastic moduli heterogeneity.

Several combinations of confining stress σ_c and pore pressure P_p were selected. The σ_c and P_p were both designed to increase from 2MPa to 50MPa by 2MPa of intervals.

4.2 Stress dependent elastic moduli of clay

Mondol et al. (2008) show that elastic moduli of clay minerals are stress dependent via the measurement of the density, P-wave and S-wave velocities of kaolinite saturated in brine and subjected to confining stress. They found the density of kaolinite increased from 2.20 (g/cm^3) to 2.52 (g/cm^3), P-wave velocities increased from 1,697(m/s) to 2,470(m/s), and S-wave velocities increased from 535(m/s) to 1,014(m/s) when the confining stress increasing from 5 MPa to 50 MPa. According to experimental results from Mondol et al. (2008), the shear modulus of kaolinite under confining stress from 5 MPa to 50 MPa can be determined as from 0.88 GPa to 2.74 GPa. The shear modulus of clay μ_c (GPa) at different location, which is essential input parameter of our DCSM, under different confining stress (radial stress σ_r (GPa) in our DCSM) can be evaluated

using Eq. (17). This equation was obtained via curve fitting of the testing results of Mondol et al. (2008).

$$\mu_c = -0.92 \times 10^2 \cdot \sigma_r^2 + 9.2 \times 10^1 \cdot \sigma_r + 4.65 \times 10^{-1} \quad 0 \leq \sigma_r \leq 0.05\text{GPa} \tag{17a}$$

$$\mu_c = \mu_{c,max} \qquad \sigma_r > 0.05\text{GPa} \tag{17b}$$

In Eq. (17), $\mu_{c,max}$ is 2.76 GPa (Substitute $\sigma_r = 0.05$ GPa into Eq. (17a)) which represents the maximum value of shear modulus of clay. When $\sigma_r = 0$ GPa, a minimum shear modulus of clay ($\mu_{c,min}$) will be determined as 0.46 GPa using Eq. (17a). The stress dependent shear modulus documented by Mondol et al. (2008) and the curve fitting result was shown in Fig. 5 (circles and dashed line, respectively). The determined Poisson's ratio ν of clay is ranging from 0.44 to 0.39 based on the testing results of Mondol et al. (2008). Since the stress dependency of Poisson's ratio of clay is insignificant comparing with the stress dependency of shear modulus of clay (varied from 0.88 GPa to 2.74 GPa), we keep the stress dependent shear modulus for modelling only and the Poisson's ratio is assumed as constant. In this study, the Poisson's ratio of clay was set to be 0.25, which is identical to the one used in the simulation of CSM (Al-Wardy and Zimmerman, 2004) for comparison.

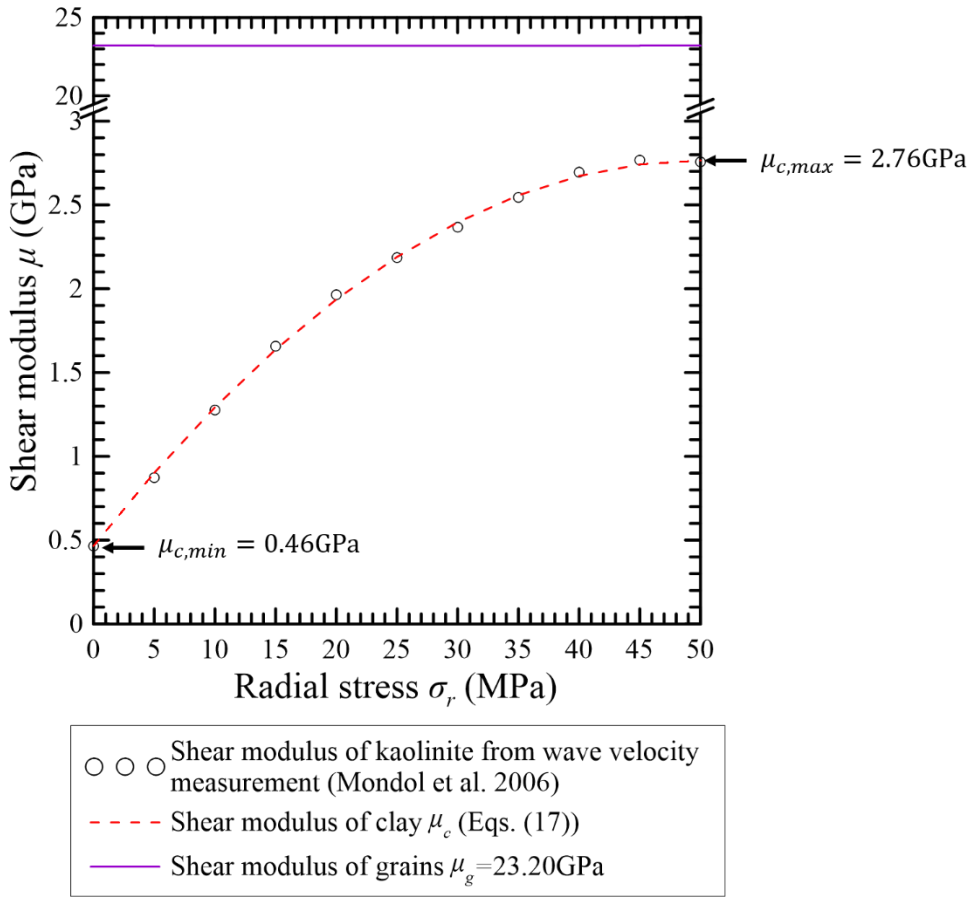

Figure 5. Stress dependent shear modulus of clay. Circles denote the shear modulus of kaolinite calculated from wave measurement (Mondol et al., 2008). Dashed red line denotes the stress dependent shear modulus of clay (μ_c) using curve fitting (Eq. (17)). Purple solid line denotes the shear modulus of grains (μ_g) which is stress independent (a constant, equals to 23.2GPa).

4.3 Elastic moduli of grains

In this study, we assume the elastic moduli of sand grains is stress independent. To compare our result to CSM (Fig. 2), the shear modulus of grains μ_g is 23.2GPa (illustrated in Fig. 5 together with the one of clay, μ_c) which is 50 times larger than the minimum shear modulus of clay $\mu_{c,min}$. That is, the shear modulus ratio $\gamma = 50$ when the radial stress equal to zero. The Poisson's ratio of grains ν_g equals to 0.25, which is also identical to the one of CSM.

5 Results

5.1 Comparison of the α determined by CSM and DCSM (elastic moduli are stress independent)

To verify the proposed DCSM, this study compared the α documented by Al-Wardy and Zimmerman (2004) using CSM and the one calculated by the proposed DCSM, which the stress dependent moduli of clay is neglected. The parameters used are identical the one used by Al-Wardy and Zimmerman (2004). The porosity ϕ of clayey sandstone is 0.2. The Poisson's ratios ν of clay and grains are 0.25, the shear modulus of grains μ_g is 23.2GPa.

Figure 6 show the predicted α varied with clay fraction using CSM (dashed lines) and proposed DCSM (circles). For shear modulus ratio γ ($=\frac{\mu_g}{\mu_c}$) equals to 50, the shear modulus of clay μ_c is 0.46GPa. For shear modulus ratio γ equals to 25, the shear modulus of clay μ_c is 0.92GPa in DCSM (The shear modulus of grain remains as 23.2 GPa, according to Fig. 5). The comparison shows the DCSM yields identical results of α predicted by CSM when the elastic moduli of clay assumed as stress-independent.

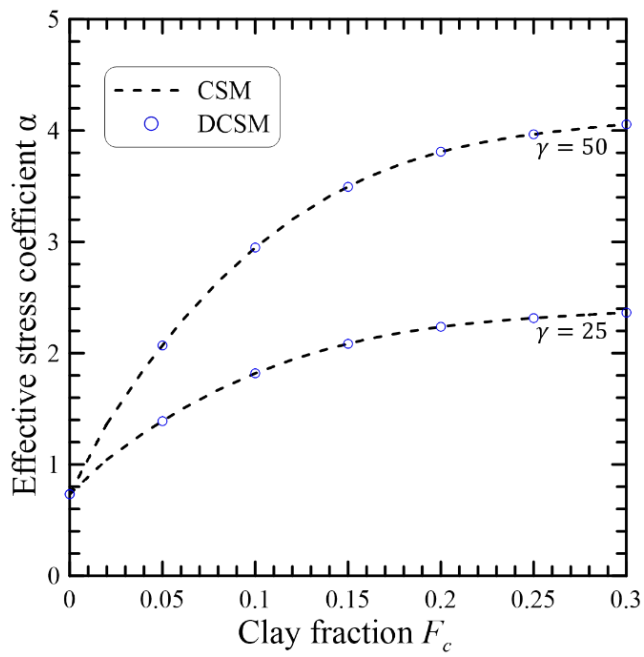

Figure 6. Comparison of the α determined by CSM (Clay Shell Model) and the proposed DCSM.

The dashed lines represent the effective stress coefficient α predicted by CSM when the shear modulus ratio $\gamma = 25$ and 50 (shown in Fig. 2 previously). The circles are the calculated α using the proposed DCSM. The parameters used are identical to ones used by Al-Wardy and Zimmerman (2004). The $\mu_g = 23.2$GPa. When $\gamma = 25$, $\mu_c = 0.92$GPa. When $\gamma = 50$, $\mu_c = 0.46$GPa.

5.2 Three different stress-dependent shear modulus of clay with different stress sensitivity

To account for the influence of stress dependent elastic moduli of clay to α, this study using Eq. (17) to depict the stress dependent shear modulus of clay on DCSM. This study designed three different stress dependent models of clay shear modulus with different stress sensitivity. These three models depict different consolidation degree of clay coating on the sand grains of clayey sandstones. Fig. 7(a) shows the three stress-dependent shear moduli of Clay 1, 2, 3. The maximum shear modulus ($\mu_{c,max}$) of each clay model is 2.76 GPa. Red dashed line is Clay 1, with $\mu_{c,min} = 0.46$GPa. Blue dashed line is Clay 2, with $\mu_{c,min} = 1.26$GPa. Green dashed line is Clay 3, with $\mu_{c,min} = 2.26$GPa. The stress sensitivity of shear modulus decreased from Clay 1 to Clay 3 and this could relate to the consolidation degree of clay filled in the voids of sand grains. Notable, the curve of Clay 1 is identical to the curve shown in Fig. 5, which is the testing results of kaolinite powder from Mondol et al. (2008).

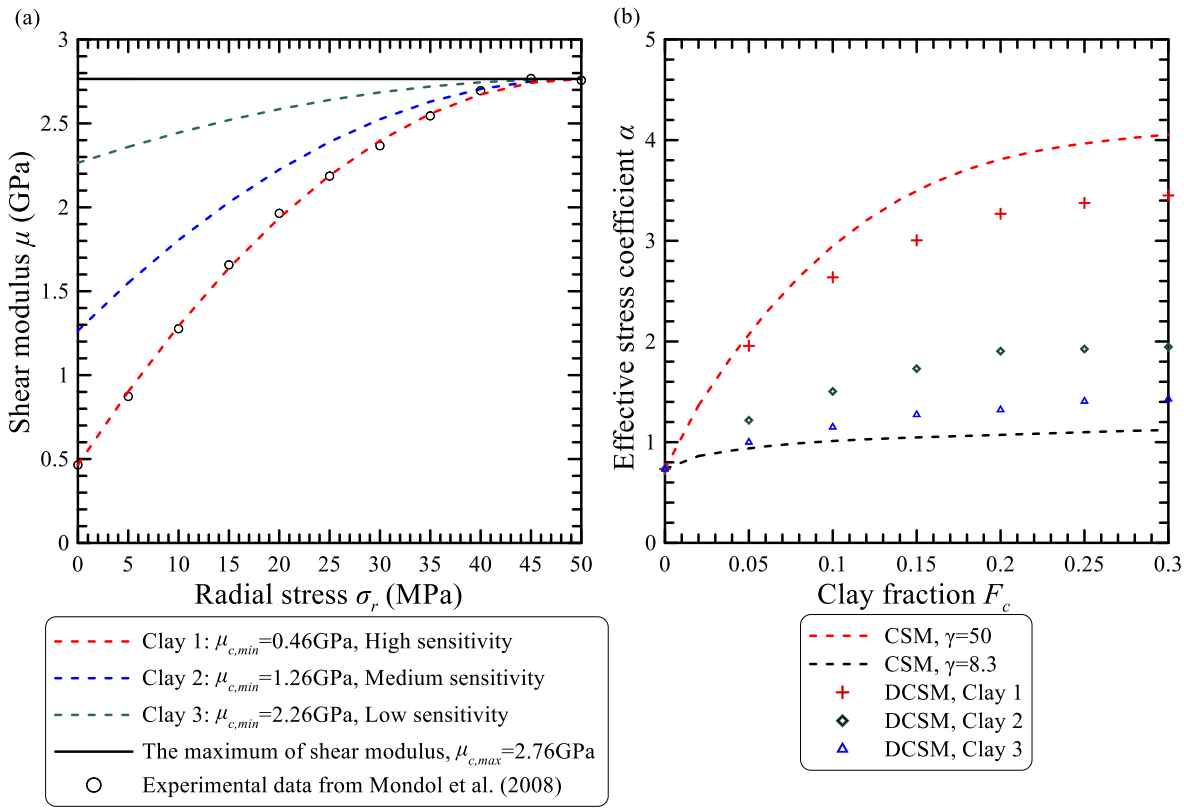

Figure 7. (**a**) Different stress sensitivity of clay shear modulus. The maximum of shear modulus ($\mu_{c,max}$) all maintain at 2.76GPa. The $\mu_{c,min}$ of Clay 1, 2, 3 are 0.46GPa, 1.26GPa, and 2.26GPa, respectively; (**b**) The predicted α with $\sigma_c = 50$ MPa and $P_p = 0$ MPa using DCSM assigning shear moduli of Clay 1, 2, 3 with different stress sensitivity. The porosity (ϕ) of clayey sandstone is assumed as 0.2; The shear modulus of grains $\mu_g = 23.20$GPa, the Poisson's ratios of clay and grains (ν) are 0.25. The predicted α for $\gamma = 50$ ($\mu_c = 0.46$ GPa, $\gamma = \frac{\mu_g}{\mu_c}$) and $\gamma = 8.3$ ($\mu_c = 2.76$GPa, $\gamma = \frac{\mu_g}{\mu_c}$) using CSM was provided for comparison.

Figure 7(b) depicts the influences of stress dependent shear modulus on α under specific stress condition with $\sigma_c = 50$MPa and $P_p = 0$ MPa. The values of clayey sandstone porosity, the shear modulus of grains, the Poisson's ratios of clay and grains are identical to ones used in Section 5.1. The cross, diamond, and triangle symbols represent the predicted α for Clay 1, 2, and 3, respectively. Again, when $F_c = 0$, the effective stress coefficient α is 0.73 for all clay model which fits the analytical solution of CSM for clean sandstones. When F_c increases from 0 to 0.3, the α

increases from 0.73 to 3.45 for Clay 1 (crosses in Fig. 7(b)). The predicted α for $\gamma = 50$ ($\mu_c = 0.46$ GPa) and $\gamma = 8.3$ ($\mu_c = 2.76$ GPa) using CSM was illustrated in dashed lines of Fig. 7(b). These two lines are upper and lower bounds of α for Clay 1 since the minimum and maximum shear moduli of Clay 1 are 0.46GPa and 2.76GPa, respectively.

When the stress sensitivity of clay shear modulus decreased (Clay 2 and Clay 3), the α decreases accordingly. When F_c equals to 0.3, the α is 1.97 and 1.43 for Clay 2 (diamonds in Fig. 7(b)) and Clay 3 (triangles in Fig. 7(b)), respectively. These values are smaller than the one for Clay 1 (α =3.45 when F_c =0.3). This result indicates that CSM failed to make a precise prediction if the shear modulus of clay is stress dependent with different sensitive. Moreover, the sensitivity of α to the clay fraction will be influenced by the stress dependent model of shear modulus.

Please note that the α predicted by DCSM can vary with σ_c and P_p, the boundary conditions used should be specified when comparing with CSM. The influence of different stress condition (combination of σ_c and P_p) will be elaborated further in Section 5.3.

5.3 Confining stress / pore pressure dependency of α

This section shows the unique results produced by DCSM, considering the influence of confining stress and pore pressure on α. Figure 8 shows the predicted effective stress coefficient α by CSM is irrelevant to the confining stress σ_c and pore pressure P_p. The predicted α equals to 4.05 when the clay fraction $F_c = 0.3$ and $\gamma = 50$, which can be read from Fig. 6.

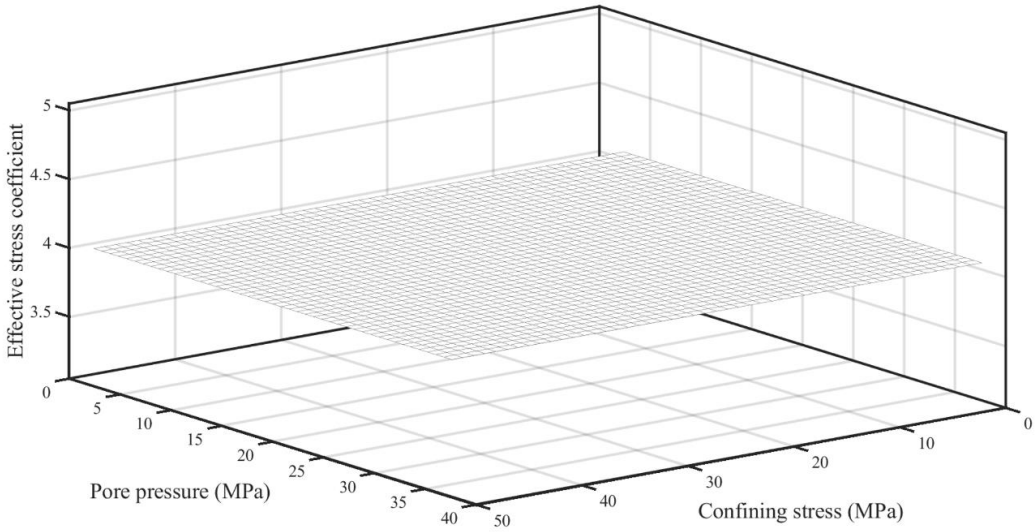

Figure 8. The effective stress coefficient α of clayey sandstones predicted by CSM is pore pressure/confining stress – independent. This plot shows the α equals to 4.05 with clay fraction $F_c = 0.3$ and $\gamma = 50$, which can be read from Fig. 6.

Figure 9(a) shows the surface depicting the stress dependent effective stress coefficient $\alpha_{(\sigma_c,P_p)}$ versus σ_c and P_p (Clay 1, ϕ=0.2, $F_c = 0.3$, Poisson's ratio of clay and grain ν=0.25). The red vertical planes in Fig. 9(a) represents the conditions where the pore pressure P_p equals to the confining stress σ_c. This study only focuses on the conditions where P_p lower than σ_c. To visualize the influence of P_p and σ_c on α two dimensionally, Fig. 9(b) shows the contours of Fig. 9(a). Figure 9(c) shows the relation between $\alpha_{(\sigma_c,P_p)}$ and σ_c when P_p remains unchanged (10, 20, 30 MPa). Figure 9(d) shows the $\alpha_{(\sigma_c,P_p)}$ under different P_p when σ_c=30, 40, 50 MPa.

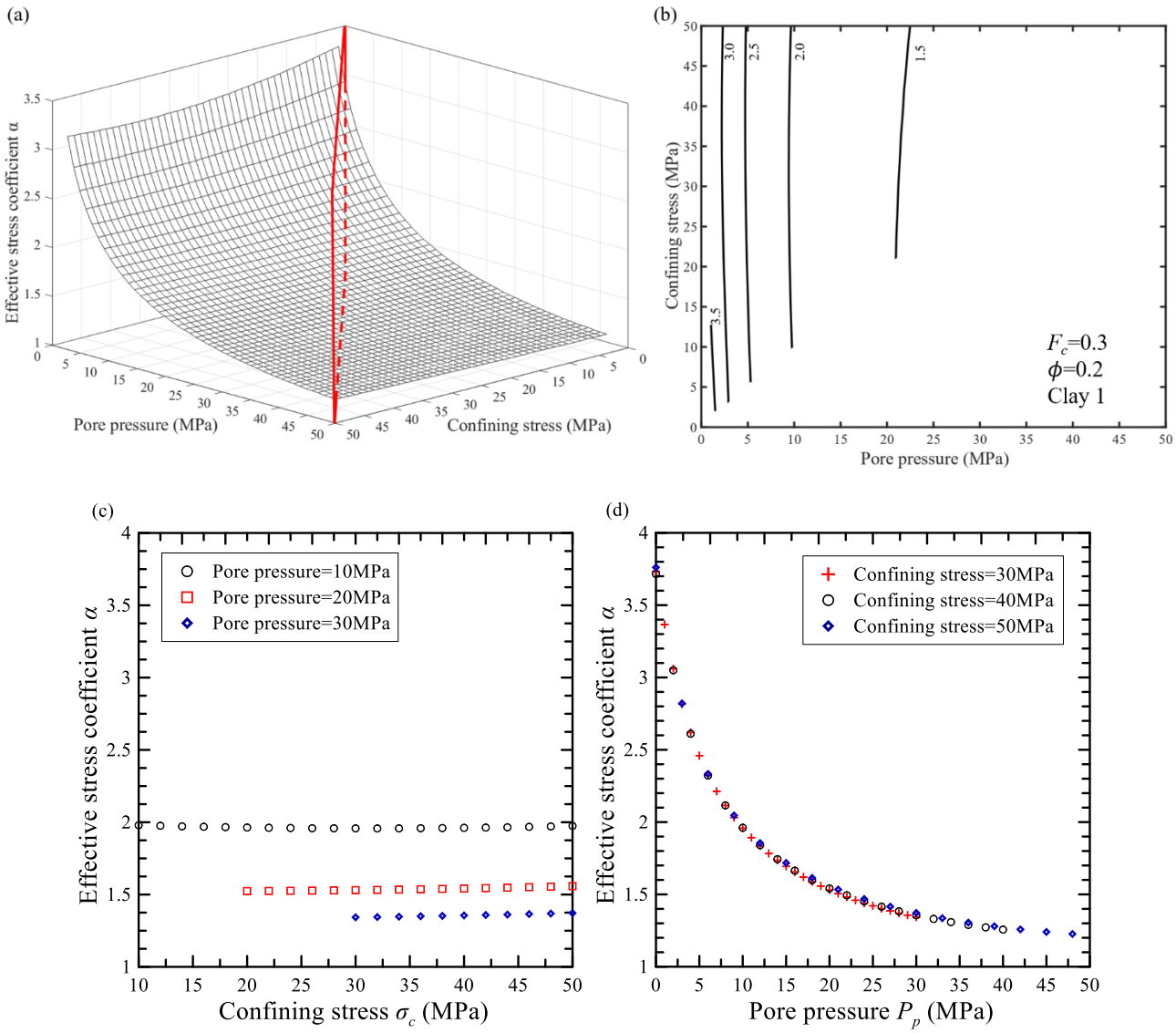

Figure 9. (**a**) The effective stress coefficient α of clayey sandstones (Clay 1, ϕ=0.2, $F_c = 0.3$, Poisson's ratio of clay and grains $\upsilon = 0.25$) predicted by the proposed DCSM is pore pressure/confining stress – dependent. The red vertical planes representing the conditions where the pore pressure P_p equals to the confining stress σ_c; (**b**) The contours of stress coefficient α derived from the surface shown in Fig. 10(a); (**c**) The α changes with the confining stress. Black circles, red squares and blue diamonds denote the α changes with the pore pressure when the confining stress is 10MPa, 20MPa, and 30MPa, respectively; (**d**) The α changes with the pore pressure. Red cross and black circles, and blue diamonds denote the α changes with the pore pressure when the confining stress is 30MPa, 40MPa and 50MPa, respectively.

Figure 9(b) shows the contours are almost parallel to the y-axis when pore pressure is lower than 15MPa. It indicates the influence of confining stress on the effective stress coefficient α is relatively minor. This can be read from Fig. 9(c), too. Figure 9(d) shows the α is significantly influenced by pore pressure. When the pore pressure is lower than 1MPa, the α can be as high as 3.70 but the α decreases rapidly with increasing pore pressure (Fig. 9(d)). When pore pressure is larger than 25MPa, the α will be less than 1.5.

5.4 Dominating factors on effective stress coefficient $\alpha_{(\sigma_c,P_p)}$ under different stress combinations (σ_c and P_p).

This section tries to illustrate the influence of different factors considered in the proposed DCSM on effective stress coefficient α. Three factors are analyzed: (1) clay fraction F_c; (2) stress dependent shear modulus the clay (Clay l, Clay 2, and Clay 3 in Fig. 7(a)); and (3) porosity ϕ, under different combination of confining stress σ_c and pore pressure P_p.

5.4.1 Influence of clay fraction on $\alpha_{(\sigma_c,P_p)}$

Figures 10 shows the influence of clay fraction (F_c) on α, which the coating material on grain is Clay 1 (high stress sensitivity) with ϕ=0.2. Firstly, the contours of effective stress coefficient α of Fig. 10(a), 10(b), and 10(c) are sub-vertical. This implies the effective stress coefficient α will not change significantly when the confining stress (vertical axis) varied. Secondly, when the pore pressure increases, the contours lines start to deviate from the vertical. However, the spacing of the contours line are not equal. With increasing pore pressure, the spacing of contours line will increase. That means, the pore pressure influence on the α will reduce. Finally, under same confining stress and pore pressure, the α decreases with decreasing clay fraction F_c. For example, when $F_c = 0.3$, the α changes from about 2.5 to larger than 1.5 under the pore pressure from 5 MPa to 20 MPa. Under same pore pressure, the α changes from smaller than 2 to about 1.25 when $F_c = 0.1$.

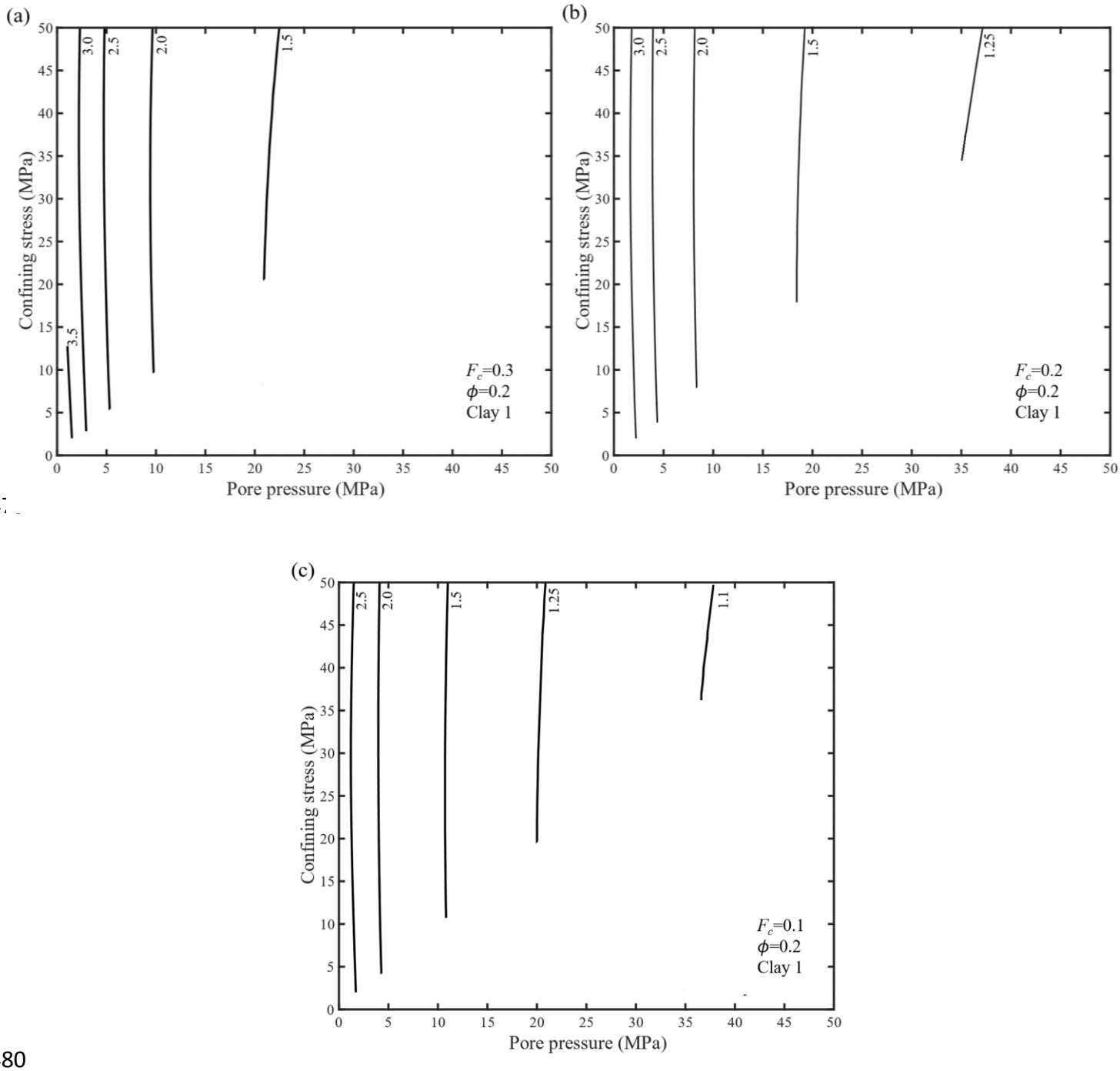

Figure 10. The contours of effective stress coefficient α versus confining stress σ_c and pore pressure P_p of the clayey sandstones for different clay fraction (F_c). The porosity ϕ=0.2, Poisson's ratio of clay and grains $\upsilon = 0.25$, the shear modulus of grains μ_g=23.2GPa. (**a**) $F_c = 0.3$, Clay 1 (refer to Fig. 8(a) which $\mu_{c,max} = 2.76$GPa, and $\mu_{c,min} = 0.46$GPa); (**b**) $F_c = 0.2$, Clay 1; (**c**) $F_c = 0.1$, Clay 1.

5.4.2 Influence of stress dependent shear modulus of clay on $\alpha_{(\sigma_c, P_p)}$

The stress dependent shear moduli of different clay materials (Clay 1-3) and their influence on the effective stress coefficient α under σ_c=50 MPa and pore pressure P_p=0 has already been illustrated in Figs. 7(a) and 7(b). This section tries to depict the combined effect of pore pressure, confining stress, and the stress dependency of different clay materials on the effective stress coefficient α (Fig. 11(a) for Clay 1, Fig. 11(b) for Clay 2, and Fig. 11(c) for Clay 3). In all figures, the clay fraction F_c is assumed to be 0.3 and the porosity ϕ is 0.2.

The contours of effective stress coefficient α for Clay 1 and 2 are sub-vertical (Figs. 11(a) and 11(b)) generally still, as illustrated in Figs. 10(a), 10(b), 10(c). That is, the influence of confining stress is insignificant compare to the one of pore pressure. It seems that the contours lines in Fig. 11(c) deviated from sub-vertical. However, the contour values of α is within a narrow range (1.24-1.40). This implies the lower stress dependency of shear modulus of clay yield lower pore pressure dependent α. Moreover, the α decreases with decreasing stress sensitivity of moduli under same confining stress and pore pressure. For Clay 1, the α changes from about 2.5 to larger than 1.5 under the pore pressure from 5 MPa to 20MPa (Fig. 11(a)). Under the same pore pressure, the α changed from about 1.36 to about 1.28 for Clay 3 (Fig. 11(c)). Similar to Fig. 10, the spacing of the contours line are increased with increasing pore pressure and the influence of pore pressure on α will reduce accordingly.

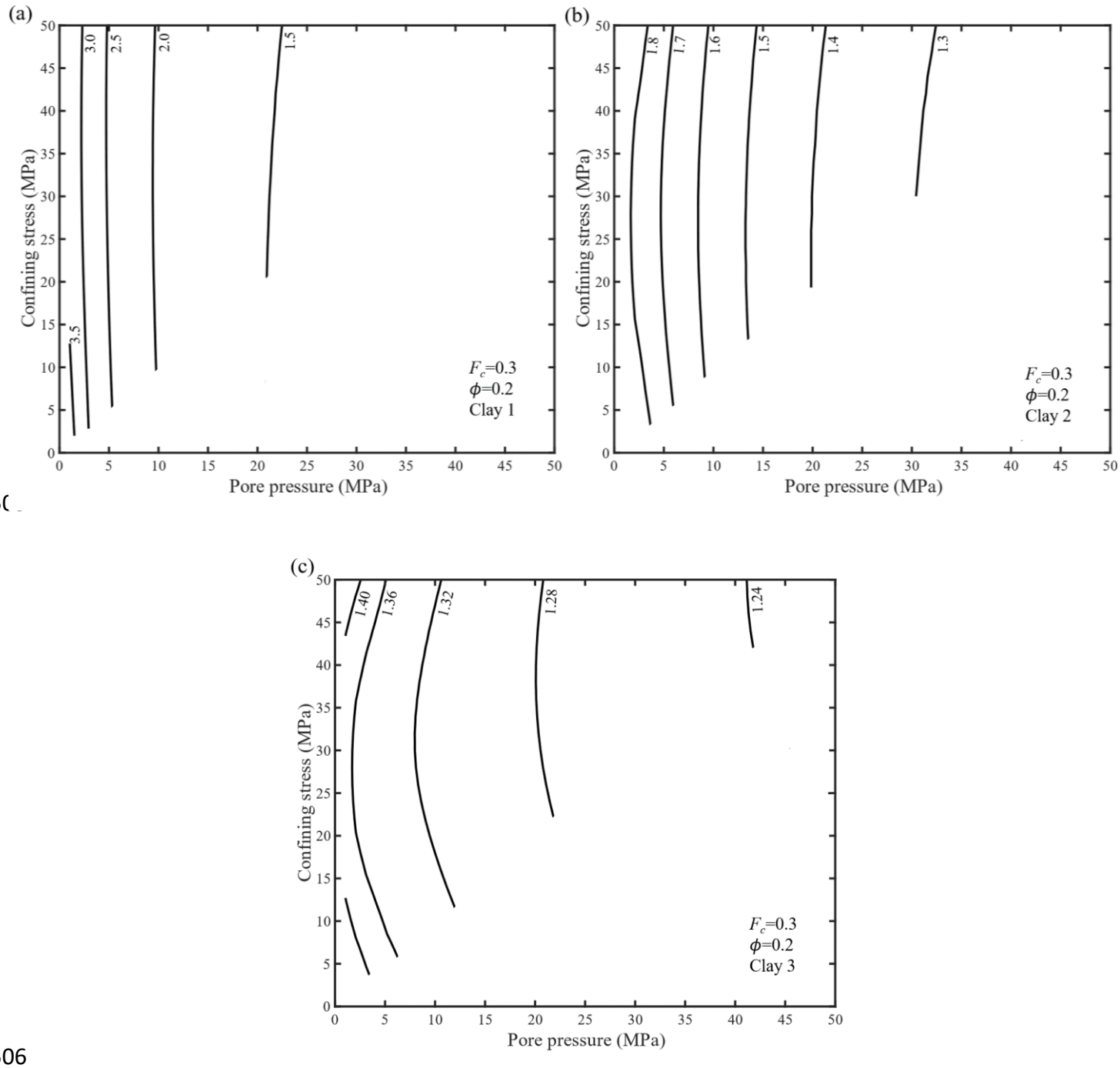

Figure 11. The contours of effective stress coefficient α versus confining stress σ_c and pore pressure P_p of the clayey sandstones for different Clay model (refers to Fig. 7(a)). The fraction of clay $F_c = 0.3$, the porosity ϕ=0.2, the Poisson's ratio of clay and grains $\nu = 0.25$, and the shear modulus of grains μ_g=23.2GPa. (**a**) Clay 1: The $\mu_{c,max} = 2.76$GPa and $\mu_{c,min} = 0.46$GPa; (**b**) Clay 2: The $\mu_{c,max} = 2.76$GPa and $\mu_{c,min} = 1.26$GPa.; (**c**) Clay 3: The $\mu_{c,max} = 2.76$GPa and $\mu_{c,min} = 2.26$GPa.

5.4.3 Influence of porosity on $\alpha_{(\sigma_c, P_p)}$

Figures 12(a) and 12(b) show the difference of predicted α of clayey sandstones when the porosity ϕ equals to 0.20 and 0.10, respectively. The clay model is Clay 1 with F_c=0.3. We find that the α increases with decreasing porosity under same stress condition. For ϕ=0.20, the contour values of α ranges from 3.6 to 1.6 (Fig. 12(a)). For ϕ=0.10, the contour values of α ranges from 5.0 to 1.8 (Fig. 12(b)). Again, the confining stress has insignificant effect on α.

It is interesting to note that lower porosity yields higher pore pressure sensitivity (denser spacing of contour lines). Please note that when the clay fraction is fixed, the lower porosity indicating thicker clay domain. Increasing the thickness of clay domain results in increasing effective stress coefficient α, if the radii of pore and outer ring of grain keep unchanged. This is the case for Al-Wardy and Zimmerman (2004) when the porosity keep as constant and clay fraction (F_c) increased. To conclude, the effective stress coefficient α is influenced by the ratio of three parameters, radii of pore, outer ring of grain, and clay domain thickness. Without the consideration of combining effect of clay fraction and porosity, the explanation could be misleading.

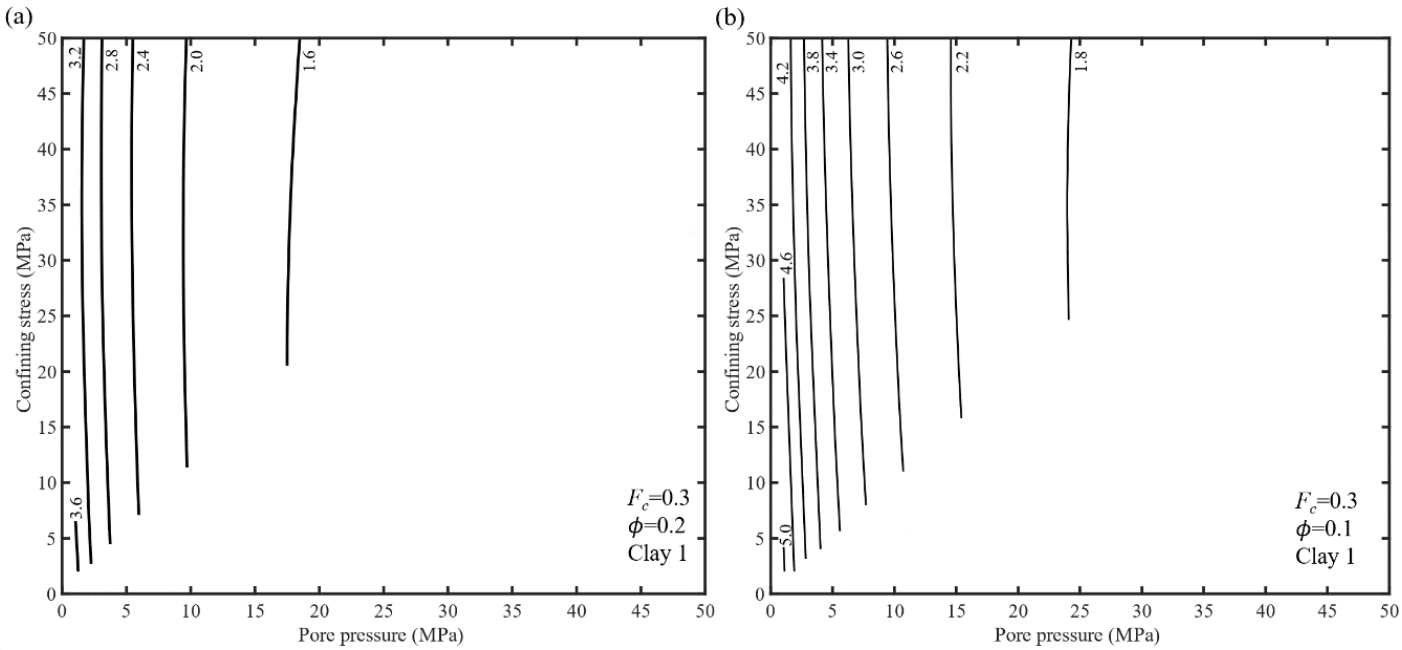

Figure 12. The contours of effective stress coefficient α versus confining stress σ_c and pore pressure P_p of the clayey sandstones for different porosity (ϕ). The Poisson's ratio of clay and grains $\nu = 0.25$. The shear modulus of grains μ_g=23.2GPa. The clay fraction $F_c = 0.3$ and the coating clay is Clay 1. (**a**) ϕ=0.2; and (**b**) ϕ=0.10.

6 Discussions

6.1 The controversial measurement results of α for clayey sandstones

6.1.1 Should the α increase or decrease with increasing confining stress?

Quite a lot of experimental results shows the α of clayey sandstones decrease with increasing confining stress (e.g. Siggins and Dewhurst, 2003; Abass, et al., 2009; Dassanayake et al., 2015; Ingraham et al., 2017) when the pore pressure is fixed at constant. On the contrary, Ghabezloo et al. (2009) found the α of limestone (clay coating on the pore wall) increase with increasing confining stress. These controversial results can be explained by the different combination of pore pressure and confining stress. In Fig. 11(c) (for Clay 3, consolidation degree of clay is high and low stress

sensitivity), the α will increase with increasing confining stress when the confining stress below certain threshold (~25 MPa when the pore pressure fixed at 5MPa). Based on Fig. 11(c), we illustrate the α varied with confining stress under constant pore pressure (5 MPa, 10 MPa, and 15 MPa) in Fig. 13. When pore pressure=5MPa (Black crosses), the α decreases with increasing confining stress first. When confining stress goes up to a critical confining stress (30 MPa), the α starts to increase with increasing confining stress. The α will decreased with increasing pore pressure (Blue squares and red circles). Moreover, the critical confining stress (trend of α vs confining stress changed) increased when pore pressure elevated. It is interesting to note that under low pore pressure, the trend of α with increasing confining stress when the confining stress goes up beyond the critical value become insignificant. Please note that, the observed trend will dominate by other variables such as stress dependence of elastic modulus of clay, porosity, clay fraction, etc.

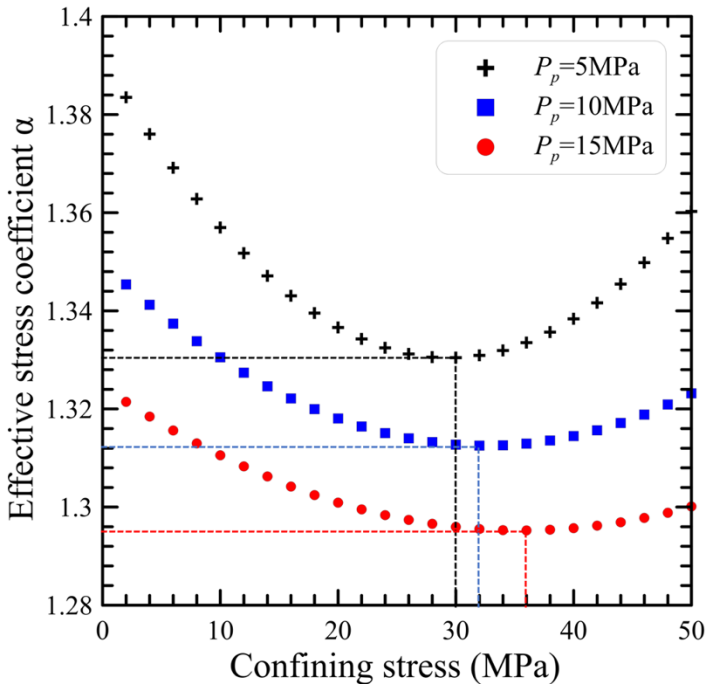

Figure 13. For Clay 3 (high consolidation), porosity is 0.2, and clay fraction is 0.3. The effective stress coefficient α would increase with increasing confining stress but lower than 25MPa at fixed pore pressure. When the confining stress beyond the 25MPa, α would decrease with increasing confining stress at fixed pore pressure.

6.1.2 Can differential pressure be used to predict α?

Some previous studies (e.g., Siggins and Dewhurst, 2003; Abass, et al., 2009) used differential pressure σ_d (confining stress minus pore pressure) to evaluate the effective stress coefficient α. This could oversimplify the combining effect of confining stress and pore pressure on α. Using the calculated contours of α in Fig. 11(c) as an example (Fig. 14), the iso-differential pressure (σ_d) lines (two gray dashed lines) intersected with different contour lines of α, indicating that the differential pressure σ_d could not be a single quantity to evaluate the effective stress coefficient α. However, it is interesting to observed that when the σ_d increased from 5MPa to 45MPa, the variation of α along the iso- differential pressure (σ_d) lines reduced significantly. It indicates that when the differential pressure increased, the simplification to use σ_d for evaluating α could induce minor errors.

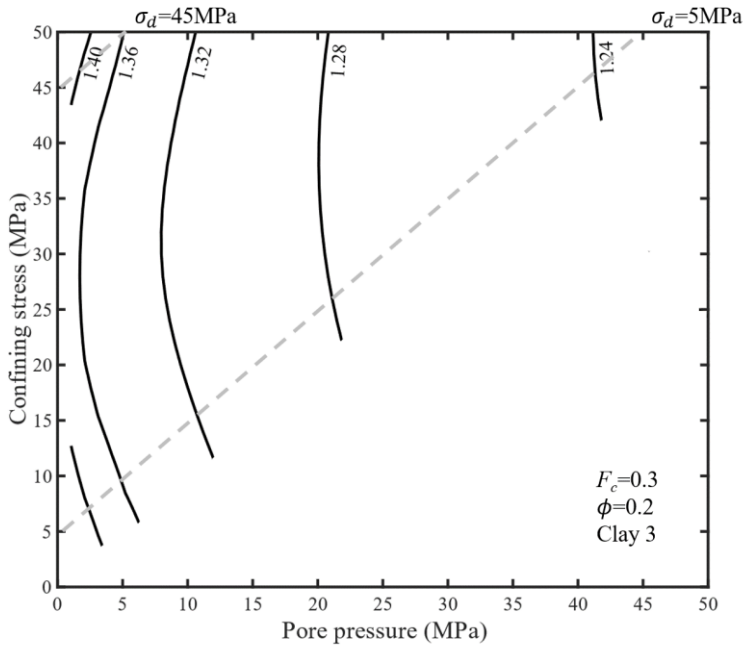

Figure 14. The contours of effective stress coefficient α shown in Fig. 11(c). The dashed line represents the iso-differential stress σ_d, which are 5MPa and 45MPa, respectively.

6.1.3 Why the $\alpha < 1$ for some high clay content sandstones?

Al-Wardy and Zimmerman (2004) found the α could be up to 5.5 for Stainton sandstone. However, the α measured in some previous studies (e.g. Ingraham et al., 2017) were smaller than 1 even the clay fraction approach to 20%. The quantitative evaluation of clay content could be an arguable point. Al-Wardy and Zimmerman (2004) use SEM to identify the clay fraction but the Laser Particle Size Analyzer (LPSA) was used by Ingraham et al. (2017). The SEM image can appropriately evaluate the content of clay coating on the pore wall. However, the clay content characterized by the LPSA cannot guarantee the presence of clay is coated on the pore wall. We suspect the high clay content identified by LPSA could include the grains which contain clay mineral, together with the clay filled within the pores (which should be used to evaluate the clay fraction F_c of CSM and DCSM). That is, the clay fraction (parameters of CSM and DCSM) of the clayey sandstones which documented by the papers showing $\alpha < 1$ could be lower than expected. It has already been indicated that the predicted effective stress coefficient α via CSM could be lower than 1 when the clay fraction is low enough (Fig. 2). Our DCSM predicted α of clayey sandstones below 1 as well (Fig. 15) if the clay fraction is low enough (F_c=0.05) and high consolidation degree (Clay 3, high value and low stress sensitivity of clay shear modulus) clay filled within the pores.

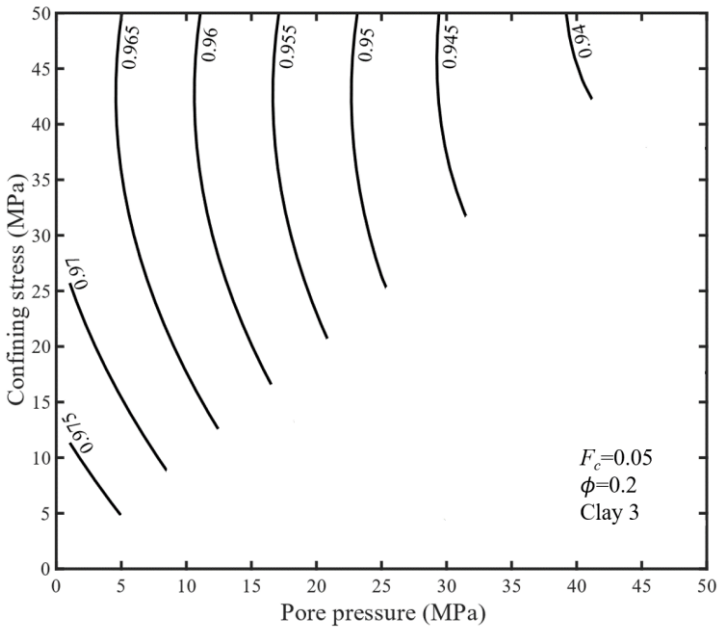

Figure 15. The contours of effective stress coefficient α is always below 1 when $F_c = 0.05$ (low clay fraction) and Clay 3 (high consolidation degree with low stress sensitivity of clay shear modulus which $\mu_{c,max} = 2.76$GPa and $\mu_{c,min} = 2.26$GPa; Fig. 8(a)) was selected. The porosity of clayey sandstone ϕ=0.2; Poisson's ratio of clay and grains $\upsilon = 0.25$; the shear modulus of grains μ_g=23.2GPa.

The micro cracks within the samples could be another influential factor on the high variability of the measured α. Li et al (2009) measured the effective stress coefficient α for permeability of 23 clayey sandstones under different combinations of stress conditions. The results show α ranged from 1.33 to 0.86. However, some of the α under different σ_c and P_p could as low as 0.3. Li et al. (2009) pointed out that micro cracks broke the effectively impermeable condition of clay clumps in pore system which resulted in a low α. This statement was supported by Meng et al. (2020) who measured α of Rothbach sandstones for permeability parallel and perpendicular to bedding. The α of sample which the permeability measured parallel to bedding plane is about 1.2. However, the one measured perpendicular to bedding plane is about 0.8. It may infer that α could be anisotropic caused by micro cracks, and need more evidence to support for further study.

6.2 The influence of effective stress coefficient α on the stress dependent permeability – implications of DCSM for laboratory scale and in-situ scale

Rock permeability, basic petrophysical properties, plays an important role for the migration of fluid. Fluid flow simulation in the crust requires permeability-depth (effective stress) relation. Usually, the measurement of stress dependent permeability is under wide range of confining stress but narrow range of pore pressure (gray window in Fig. 16). Meanwhile, the pore pressure is generally low compared to the confining stress. Most of the researchers (e.g. David et al., 1994; Dong et al., 2010) assumed the effective stress coefficient is a constant (e.g., $\alpha = 1$) and plotted the testing results of permeability together with effective stress.

The stress combinations in-situ is different from laboratory tests significantly. To simplify the discussion, we assume the in-situ stress state is isotropic and the pore pressure is hydrostatic. The gray dashed line in Fig. 16 represents the stress combinations (pore pressure and confining stress) from shallow to great depth. The domain between gray and red dashed line (pore pressure equals to confining stress) represents the overpressure conditions.

The effective stress coefficients α of a hypothetical clayey sandstone under different combinations of confining stress and pore pressure are illustrated in Fig. 16 as well. The clay fraction $F_c = 0.3$, porosity ϕ=0.2, and clay type is Clay 2. It is interesting to discuss the influence of effective stress coefficient α on the estimation of stress-dependent permeability under laboratory and in-situ conditions. Base on the determined α in Fig.16, this study designed two synthetic cases in Section 6.2.1 and Section 6.2.2 to illustrate the importance for reasonably estimating the effective stress coefficient α.

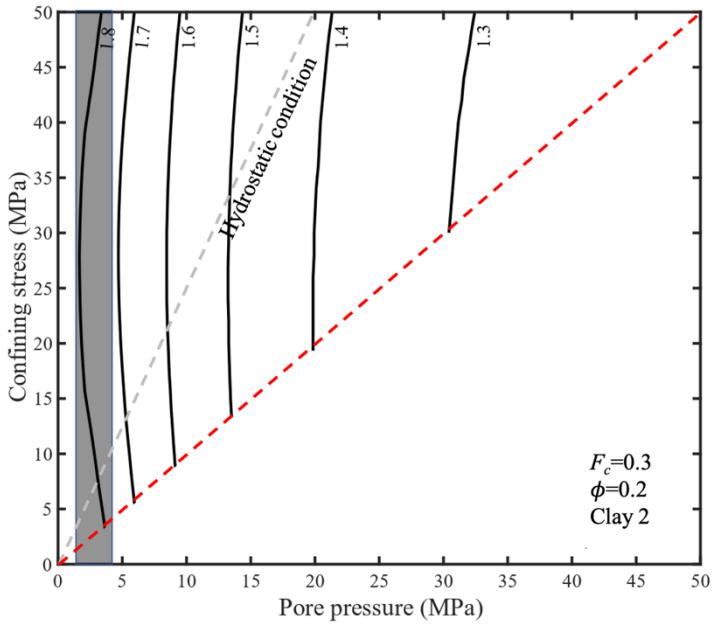

Figure 16. Stress combinations (pore pressure and confining stress) of laboratory tests (gray window; wide range of confining stress with narrow and low pore pressure) and in-situ condition (gray dashed line; hydrostatic pressure). The domain between gray and red dashed line (pore pressure equals to confining stress) represents the overpressure conditions. The effective stress coefficient α under different confining stress and pore pressure for clayey sandstones with clay fraction $F_c = 0.3$, porosity ϕ=0.2, and clay type is Clay 2.

6.2.1 Synthetic case of laboratory scale

This section illustrates the influence of effective stress coefficient α on the determination of material constants of effective stress dependent permeability in the stress combination range for laboratory test (gray window in Fig. 16). We provide the value of α of rock under different stress combinations (pore pressure and confining stress) based on the synthetic case shown in Fig. 16 (porosity $\phi = 0.2$, clay fraction $F_c = 0.3$, and clay type is Clay 2). Therefore, the effective stress under different stress combinations can be determined via Eq. (3). We assumed the "true" permeability can be determined using the stress dependent power law proposed by Shi and Wang

(1986) under "true" effective stress which determined from determined α (see Fig. 16, DCSM) and designed confining stresses and pore pressure. On the other hand, we used the same design confining stresses and pore pressure ("true" permeability remains unchanged therefore) but assumed $\alpha = 1$ (widely adopted by experimentalists) to calculate the "apparent" effective stress. The influence of effective stress coefficients α on the relation between effective stresses and permeabilities will be explored.

Shi and Wang (1986) suggested that the relationship between effective stress and rock permeability following a power law:

$$k = k_0 \left(\frac{\sigma_{eff}}{\sigma_0}\right)^{-p}, \tag{18}$$

where k_o is permeability at atmospheric pressure, σ_o which equals to 0.1 MPa, and p is the stress sensitivity coefficient of permeability. Dong et al. (2010) measured the permeabilities of numerous sandstones and mudrocks from Hole-A of Taiwan Chelungpu-fault Drilling Project. The range of p was from 0.120 to 1.677. We selected p=1.478 and permeability at atmospheric pressure k_o equals to 10^{-15} m^2 based on the testing results. The range of confining stress was from 5MPa to 50MPa with intervals of 5MPa, and the pore pressure was fixed at 2.5MPa.

Figure 17(a) illustrates the α under different stress combinations (determined by DCSM; Fig. 16). The range of α was from 1.77 to about 1.88 when confining stress changed from 5MPa to 50MPa under unchanged pore pressure (2.5 MPa). The determined α decreased with increasing confining stress first but went up when the confining stress larger than 30MPa. Using the determined α under designed stress combinations and Eq. (18), the permeabilities under different "true" effective stress can be evaluated. The calculated results are plotted on Fig. 17(b) (red circles). The permeability decreased from about 10^{-16} m^2 to 10^{-19} m^2 with increasing "true" effective stress.

As aforementioned, the effective stress coefficient α has been assumed as 1 frequently. We try to calculate the "apparent" effective stress under designed stress combinations assuming $\alpha = 1$ (Eq. (3)). The "true" permeability under designed stress combinations would not change even though the

true effective stresses replaced by the apparent ones when we assumed $\alpha = 1$. That is, we did not calculate the permeability under apparent effective stress using power law. The blue squares in Fig. 17(b) denote the permeability versus "apparent" effective stress assuming $\alpha = 1$. The differences of red circles and blue squares can be explained in more detail using an example. When confining stress σ_c=15 MPa and pore pressure P_p=2.5 MPa, the α can be determined as 1.81 (see Fig. 17(a)) and the "true" effective stress (σ_{eff}) will be 10.48 MPa. The permeability can be calculated to be 1.03×10^{-18} m^2 via Eq. (18) (red circle in Fig. 17(b)). However, under the same stress combination (σ_c=15 MPa and P_p=2.5 MPa), the "apparent" effective stress will be 12.5 MPa. Notably, the "true" permeability under this stress combination is unchanged (Fig. 17(b)).

From Fig. 17(b), it can be observed that the differences between the red circles and blue squares decreased with increasing effective stress σ_{eff} because the role of effective stress coefficient became insignificant when the confining stress is much higher than pore pressure. Usually, the experimentalists will calibrate the materials parameters (such as permeability at an atmosphere k_o and stress sensitivity coefficient of permeability p) using measured data points. The calibration results of blue squares using power law show that the k_o is 1.23×10^{-12} m^2 and p is 2.787 (Table 1). The calibrated k_o using apparent effective stress (assume $\alpha = 1$) is about three order of magnitude larger than the given one (10^{-15} m^2), and the calibrated p is about twice of the given one (1.478). The results show the strong impact of effective stress coefficient α on the laboratory data analysis for stress dependent permeability. The influence of α on in-situ permeability prediction will be illustrated in Section 6.2.2.

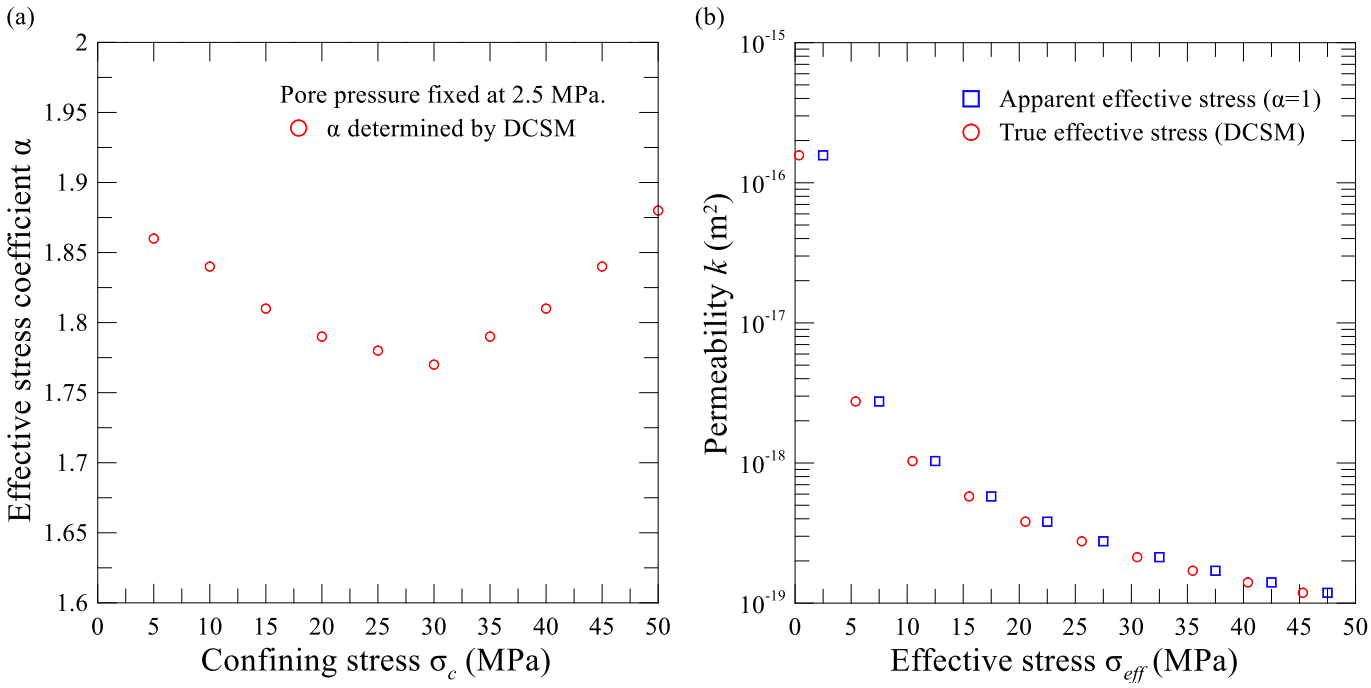

Figure 17. (a) The α determined by DCSM for designed stress combinations (confining stress and pore pressure). The range of α is from 1.77 to about 1.88 when confining stress changed from 5 MPa to 50 MPa and pore pressure held as constant (2.5 MPa). **(b)** Red circles denote the relationship between "true" effective stress and permeability calculated from power law. The blue squares denote the permeability under different "apparent" effective stress.

Table 1. Given material constants (k_o and p) and calibrated ones using data points of "apparent" effective stress and true permeability.

	Power law $^{*}k = k_0\left(\frac{\sigma_{eff}}{\sigma_0}\right)^{-p}$		
	k_0 (m^2)	p	R^2
k_0 and p for calculating true permeability using true effective stress calculated from α (DCSM)	10^{-15}	1.478	-
Calibrated k_0 and p using apparent effective stress assuming $\alpha = 1$	1.23×10^{-12}	2.787	0.999

$^{*}\sigma_{eff}$ is effective stress, σ_0 is an atmosphere (0.1 MPa in this study)

6.2.2 Synthetic case of in-situ scale

The significance of effective stress coefficient to permeability-depth relation will be introduced here. The in-situ stress combinations follow the gray dashed line in Fig. 16 if the pore pressure P_p is hydrostatic. Overpressure conditions produce stress combination between gray and red dashed lines are out of the scope of this discussion. To simplify the discussion, we assume the in-situ stress state is isotropic and the pore pressure P_p is hydrostatic. That is, the confining stress σ_c in Eq. (3) equals to the in-situ vertical burial stress σ_v and Eq. (3) can be rewritten as:

$$\sigma_{eff} = \sigma_v - \alpha_{(\sigma_v, P_p)} \cdot P_p, \tag{19}$$

where σ_{eff} denotes the effective vertical stress (briefly "effective stress" in this section). To compute the σ_v, we assumed the unit weight of rocks $\gamma_r = 25$ (kN/m^3), and the value of σ_v at burial depth D can be calculated by $\sigma_v = \gamma_r \times D$. Fig. 18(a) shows the vertical stress and pore pressure at different burial depth. The α of the synthetic rocks (see Fig. 16 where clay fraction $F_c = 0.3$, porosity ϕ=0.2, and clay type is Clay 2 in DCSM) can be obtained along the gray dashed line in Fig. 16 and is shown in Fig. 18(b). The α dropped from 1.88 to about 1.42 from 0.2 km to 2.0 km. The in-situ condition shows wider range of α since the pore pressure range (gray dashed line in Fig. 16) is much higher than the one for laboratory testing (gray window in Fig. 16). Using the determined α under different stress combinations (σ_v and P_p), the "true" effective stress can be calculated using Eq. (19) and illustrated in Fig. 18(c) (red circles). The blue squares are the "apparent" effective stress assuming $\alpha = 1$ which is widely used when predicting the permeability-depth relation (e.g. Meng et al., 2011). Generally speaking, the "apparent" effective stresses (blue squares) are overestimated since the determined α is larger than 1. At 2 km depth, the "true" effective stress (red circle) is 21.68 MPa while the "apparent" one (blue square) is 30 MPa.

The power law of stress dependent permeability and the material constants used in Section 6.2.1 were used again (k_o=10^{-15}m^2 and p=1.478). The permeability-depth relation can be predicted using the true and apparent effective stress and illustrated in Fig. 18(d). The red circles denote the "true"

permeability and blue squares denote the "apparent" permeability which α=1 was assumed for calculation. The apparent permeability (blue squares) will be underestimated and the discrepancy between "true" and "apparent" permeability are larger at shallow depth. From Fig. 18(d), the permeability of blue squares at 100 m is about one order of magnitude larger than the one of red circle.

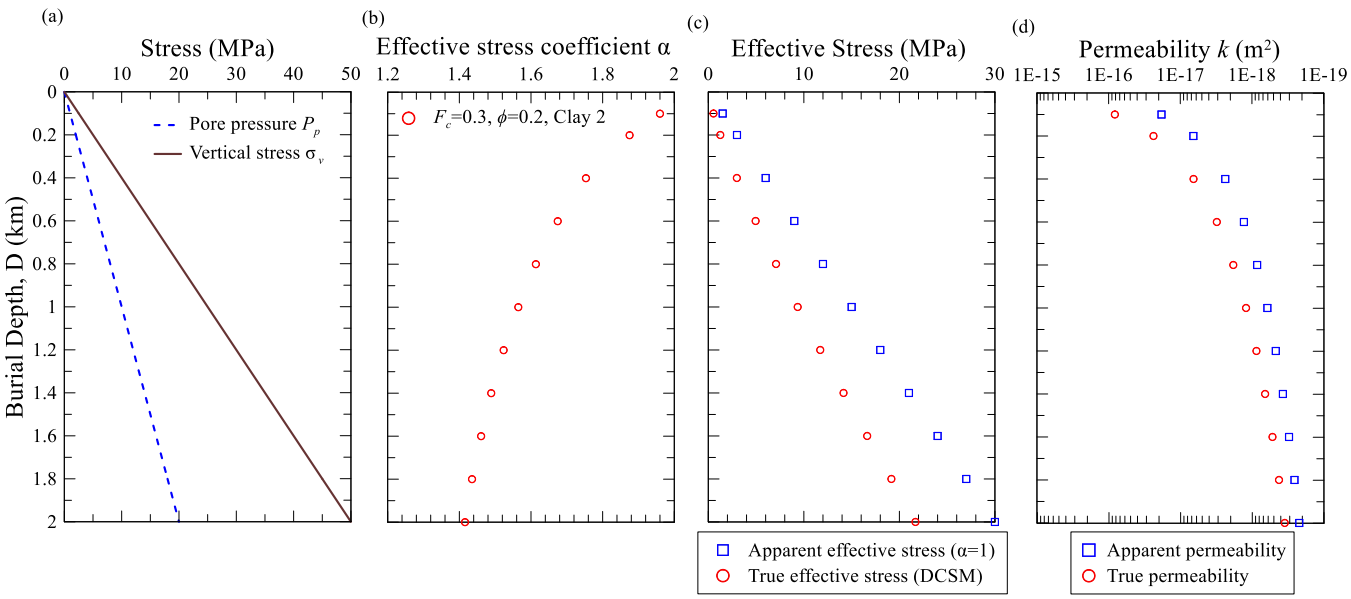

Figure 18. (**a**) Synthetic case that vertical stress σ_v and hydrostatic pore pressure p_p increased with burial depth. (Assume the average of unit weight γ_w is 25 $\mathrm{kN/m^3}$); (**b**) The effective stress coefficient α changed with burial depth determined by DCSM ($F_c = 0.3$, $\phi = 0.2$, Clay 2); (**c**) The predicted "true" effective stress by DCSM and "apparent" effective stress when $\alpha = 1$ was assumed; (**d**) The predicted permeability-depth relation based on power law (Eq. (18)). The stress sensitivity coefficient p=1.478 and permeability at atmospheric pressure k_o= $10^{-15}\mathrm{m}^2$ are identical to the ones used in Section 6.2.1. Red circles and blue squares denote the permeabilities evaluated by Eq. (18) using "true" and "apparent" effective stress.

7 Conclusions

This study modifies Clay Shell Model (CSM) by incorporating the confining stress / pore pressure dependent elastic modulus of clay into discretizing multi-layers clay domain. The proposed Discretized Clay Shell Model (DCSM) determines α under different stress conditions using iso-pore radius curves. The parametric study and the prediction of permeability-depth relation using synthetic case illustrate the superior features of the proposed DCSM to the traditional CSM. The main findings are summarized as follows:

1. The predicted effective stress coefficient α form a concaving upward surface in the pore pressure-confining stress space using DCSM while the traditional CSM yields a constant when the material properties of clay and grain remain unchanged.
2. The curvature of the concave surface of α along the pore pressure axis is smaller (flatter) than the one along the confining stress axis, indicating that the influence of pore pressure on α is stronger than the one of confining stress. When the confining stress keeping as a constant, the predicted α decreased with increasing pore pressure. The decreasing trend is stronger under low pore pressure than the one under high pore pressure. This feature can be observed from the horizontal distance between contour lines increased with increasing pore pressure. It is interesting to note that the predicted α could decrease first with elevated confining stress and start to increase when the confining stress goes up to a threshold value, if the pore pressure remains unchanged. This trend can be observed from the curved contour lines of α.
3. The stress dependent shear modulus of clay coating on the grain dominates the variability of the predicted α. When the clay was normally consolidated (Clay 1 model) and the compressibility is large, the value and variability will be large and significant. On the contrary, the predicted α of low stress sensitivity with low compressibility (Clay 3 model) will approach to 1 and the variability is lowest among the three clay model. This result indicates that the effective stress principle proposed by Terzaghi (1943) (i.e., $\alpha = 1$) can be invalidate for young, weakly cemented

clayey sandstones.

4. Same with the prediction results via CSM, the effective stress coefficient α predicted by the proposed DCSM will increase with increasing clay fraction. The predicted α could be lower than 1 for low clay content sandstones under different combination of pore pressure and confining stress. The variability of predicted α under different combination of pore pressure and confining stress using DCSM will increase when the clay fraction increased. That is, the influence of stress dependency of clay shear modulus should not be neglected when the clay fraction is high.
5. The effective stress coefficient of clayey sandstones increases with decreasing porosity when the clay fraction keep as a constant. The variation of α will increased as well when the porosity of clayey sandstones is lower. Please note that when the clay fraction is fixed, the lower porosity indicating thicker clay domain. The effective stress coefficient α is influenced by the ratio of three parameters, radii of pore, outer ring of grain, and clay domain thickness.
6. The applicability for using differential stress σ_d (Difference of confining stress and pore pressure) to predict the effective stress coefficient α depends on the combination of confining stress and pore pressure. It seems that this approach can only be valid under high confining stress, low pore pressure.
7. The determination of clay fraction of clayey sandstones should be conducted with caution. From the aspect of DCSM prediction, the SEM approach could be superior to the LPSA approach for the former one can only include the clay coating on the pore wall. The presence of micro-cracks accounts for the low measured α.
8. The significant difference of effective stress dependent permeability in synthetic laboratory test between $\alpha = 1$ and $\alpha > 1$ (based on DCSM) was observed especially under low effective stress. The calibrated parameters of power law for describing the stress dependent permeability are quite different and yield overestimated permeability up to three orders of magnitude.
9. The synthetic in-situ case shows the predicted permeability assuming α =1 could be underestimated if the true effective stress coefficient is larger than one (predicted by DCSM). The

discrepancy is increased with decreasing burial depth.

Data Availability Statement

The data published in the literatures used in this study are available through Al-Wardy and Zimmerman (2004), Mondol et al. (2008) and Dong et al. (2010), readers can find the detailed citation information in reference. All the parameters used in the equations and modeling program are explained in the text. This study complies with the AGU FAIR data policy. All the data of stress dependent effective stress coefficient with different clay fraction, porosity, and consolidation degree of clay are provided as supporting information.

Acknowledgments

This research was supported by Taiwan Ministry of Science and Technology (MOST108-2638-E-008-001-MY2 and MOST107-2116-M-008-001-MY3). This work was also financially supported by Earthquake-Disaster & Risk Evaluation and Management Center (E-DREaM) from The Featured Areas Research Center Program within the framework of the Higher Education Sprout Project by the Ministry of Education (MOE) in Taiwan.

Reference

Abass, H. H., Al-Tahini, A. M., Abousleiman, Y., & Khan, M. R. (2009). *New technique to determine Biot coefficient for stress-sensitive dual-porosity reservoirs*. Paper presented at SPE Annual Technical Conference and Exhibition, Society of Petroleum Engineers. https://doi.org/10.2118/124484-MS

Al-Wardy, W., & Zimmerman, R. W. (2004). Effective stress law for the permeability of clay-rich sandstones. *Journal of Geophysical Research, 109*(B4). https://doi.org/10.1029/2003JB002836

Bernabe, Y. (1987). The effective pressure law for permeability during pore pressure and confining pressure cycling of several crystalline rocks. *Journal of Geophysical Research, 92*(B1), 649-657. https://doi.org/10.1029/JB092iB01p00649

Berryman, J. G. (1992). Exact effective-stress rules in rock mechanics. *Physical Review A, 46*(6), 3307–3311. https://doi.org/10.1103/PhysRevA.46.3307

Box, G. P., & Draper, N. P. (1987). *Empirical Model-Building and Response Surfaces*, John Wiley, New York.

Breckels, I. M., & van Eekelen, H. A. M. (1982). Relationship between horizontal stress and depth in sedimentary basins. *Journal of Petroleum Technology, 34*, 2191-2198. https://doi.org/10.2118/10336-PA

Cao, P., Liu, J., & Leong, Y. K. (2016). General gas permeability model for porous media: bridging the gaps between conventional and unconventional natural gas reservoirs. *Energy & Fuels, 30*(7), 5492-5505. https://doi.org/10.1021/acs.energyfuels.6b00683

Civan, F., Rai, C. S., & Sondergeld, C. H. (2011). Shale-gas permeability and diffusivity inferred by improved formulation of relevant retention and transport mechanisms. *Transport in porous media, 86*(3), 925-944. https://doi.org/10.1007/s11242-010-9665-x

Coyner, K. B. (1984). Effects of stress, pore pressure and pore fluid on bulk strain, velocity, and permeability in rocks, (Doctoral dissertation). Massachusetts Institute of Technology, Cambridge, U.K.

Cui, X., Bustin, R. M., & Chikatamarla, L. (2007). Adsorption-induced coal swelling and stress: implications for methane production and acid gas sequestration into coal seams. *Journal of Geophysical Research: Solid Earth, 112*(B10). https://doi.org/10.1029/2004JB003482

Dassanayake, A. B. N.,Fujii, Y., Fukuda, D., & Kodama, J. I. (2015). A new approach to evaluate effective stress coefficient for strength in Kimachi sandstone. *Journal of Petroleum Science and Engineering, 131*, 70-79. https://doi.org/10.1016/j.petrol.2015.04.015

David, C., Wong, T. F., Zhu, W., & Zhang, J. (1994). Laboratory measurement of compaction-induced permeability change in porous rocks: implication for the generation and maintenance of pore pressure excess in the crust. *Pure and Applied Geophysics, 143*(1), 425-456. https://doi.org/10.1007/BF00874337

Dong, J. J., Hsu, J. Y., Wu, W. J., Shimamoto, T., Hung, J. H., Yeh, E. C., Wu, Y. H., & Sone, H. (2010). Stress-dependence of the permeability and porosity of sandstone and shale from TCDP Hole-A. *International Journal of Rock Mechanics and Mining Sciences, 47*(7), 1141-1157. https://doi.org/10.1016/j.ijrmms.2010.06.019

Engelder, T., & Fischer, M. P. (1994). Influence of poroelastic behavior on the magnitude of minimum horizontal stress, S_h in overpressured parts of sedimentary basins. *Geology, 22*(10), 949-952. https://doi.org/10.1130/0091-7613(1994)022<0949:IOPBOT>2.3.CO;2

Gaarenstroom, L., Tromp, R. A. J., de Jong, M. C., & Brandenburg, A. M. (1993). *Overpressures in the central North Sea: Implications for trap integrity and drilling safety*. Paper presented at Geological Society, London, Petroleum Geology Conference series. 4(1), 1305-1313. https://doi.org/10.1144/0041305

Gangi, A. F., & Carlson, R. L. (1996). An asperity-deformation model for effective pressure. *Tectonophysics, 256*, 241–251. https://doi.org/10.1016/0040-1951(95)00167-0

Ghabezloo, S., Sulem, J., Guedon, S., & Martineau, F. (2009). Effective stress law for the permeability of a limestone. *International Journal of Rock Mechanics and Mining Sciences, 46*(2), 297-306. https://doi.org/10.1016/j.ijrmms.2008.05.006

Ingraham, M. D., Bauer, S. J., Issenm K. A., & Dewers, T. A. (2017). Evolution of permeability and Biot coefficient at high mean stresses in high porosity sandstone. *International Journal of Rock Mechanics & Mining Sciences, 96*, 1–10. https://doi.org/10.1016/j.ijrmms.2017.04.004

Jaeger, J. C., & Cook N. G. W. (1979). *Fundamentals of Rock Mechanics*, Chapman and Hall, New York.

Li, M., Bernabé, Y., Xiao, W. L., Chen, Z. Y., & Liu, Z. Q. (2009). Effective pressure law for permeability of E-bei sandstones. *Journal of Geophysical Research, 114*(B07). https://doi.org/10.1029/2009JB006373

Li, M., Xiao, W. L., Bernabé, Y., & Zhao, J. Z. (2014). Nonlinear effective pressure law for permeability. *Journal of Geophysical Research: Solid Earth, 119*, 302-318. https://doi.org/10.1002/2013JB010485

Li, X., Wei, H., Chen, B., Liu, X., Wang, W., & Zhao, X. (2008). *Multi-stage fracturing stimulations improve well performance in tight oil resevoirs of the Changqing Oilfield*. Paper presented at International Petroleum Technology Conference, Kuala Lumpur, Malaysia. https://doi.org/10.2523/IPTC-12303-MS

Meng, Z., Zhang, J., & Wang, R. (2011). In-situ stress, pore pressure and stress-dependent permeability in the Southern Qinshui Basin. *International Journal of Rock Mechanics and Mining Sciences*, *48*(1), 122-131. https://doi.org/10.1016/j.ijrmms.2010.10.003

Meng, F., Li, X., Baud, P., & Wong, T. F. (2020). Bedding anisotropy and effective stress law for permeability and deformation of clayey sandstones. *Rock Mechanics and Rock Engineering*, 1-18. https://doi.org/10.1007/s00603-020-02306-w

Mondol, N. H., Jahren, J., Bjørlykke, K., & Brevik, I. (2008). Elastic properties of clay minerals. *The Leading Edge*, *27*(6), 758-770. https://doi.org/10.1190/1.2944161

Robin, P. Y. (1973). Note on effective pressure. *Journal of Geophysical Research, 78*, 2434–2437. https://doi.org/10.1029/JB078i014p02434

Shi, T. & Wang, C, Y. (1986). Pore pressure generation in sedimentary basins: overloading versus aquathermal. *Journal of Geophysical Research, 91*(B2), 2153-2162. https://doi.org/10.1029/JB091iB02p02153

Siggins, A. F. & Dewhurst, D. N. (2003). Saturation, pore pressure and effective stress from sandstone acoustic properties. *Geophysical Research Letters, 30*(2). https://doi.org/10.1029/2002GL016143

Sokolnikoff, I. S. (1956). *Mathematical Theory of Elasticity*, McGraw-Hill, New York.

Terzaghi, K. (1943). *Theoretical Soil Mechanics*, John Wiley, New York.

Todd, T., & Simmons, G. (1972). Effect of pore pressure on the velocity of compressional waves in low-porosity rocks. *Journal of Geophysical Research, 77*(20), 3731-3743. https://doi.org/10.1029/JB077i020p03731

Walls, J., & Nur, A. (1979). *Pore pressure and confining pressure dependence of permeability in sandstone*. Paper presented at the 7th Formation Evaluation Symposium of the Canadian Well Logging Society.

Warpinski, N. R., & Teufel, L. W. (1992). Determination of the effective-stress law for permeability and deformation in low-permeability rocks. *SPE formation evaluation, 7*(02), 123-131. https://doi.org/10.2118/20572-PA

Zoback, M. D., & Byerlee, J. D. (1975). Permeability and effective stress. *AAPG Bulletin, 59*(1), 154-158. https://doi.org/10.1306/83D91C40-16C7-11D7-8645000102C1865D

Figure 1.

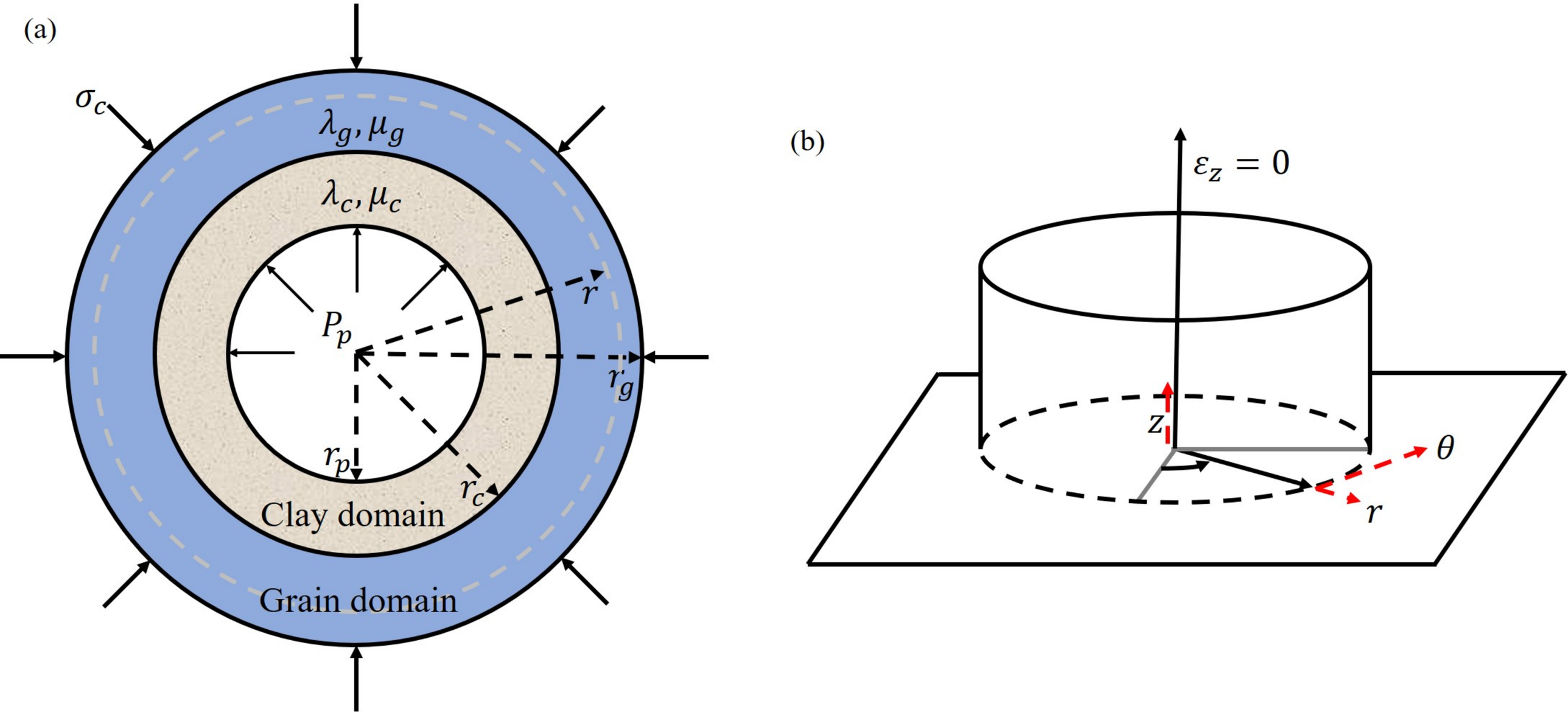
(a)
σ_c
λ_g, μ_g
λ_c, μ_c
P_p
r
r_g
r_p
r_c
Clay domain
Grain domain
(b)
$\varepsilon_z = 0$
z
θ
r

Figure 2.

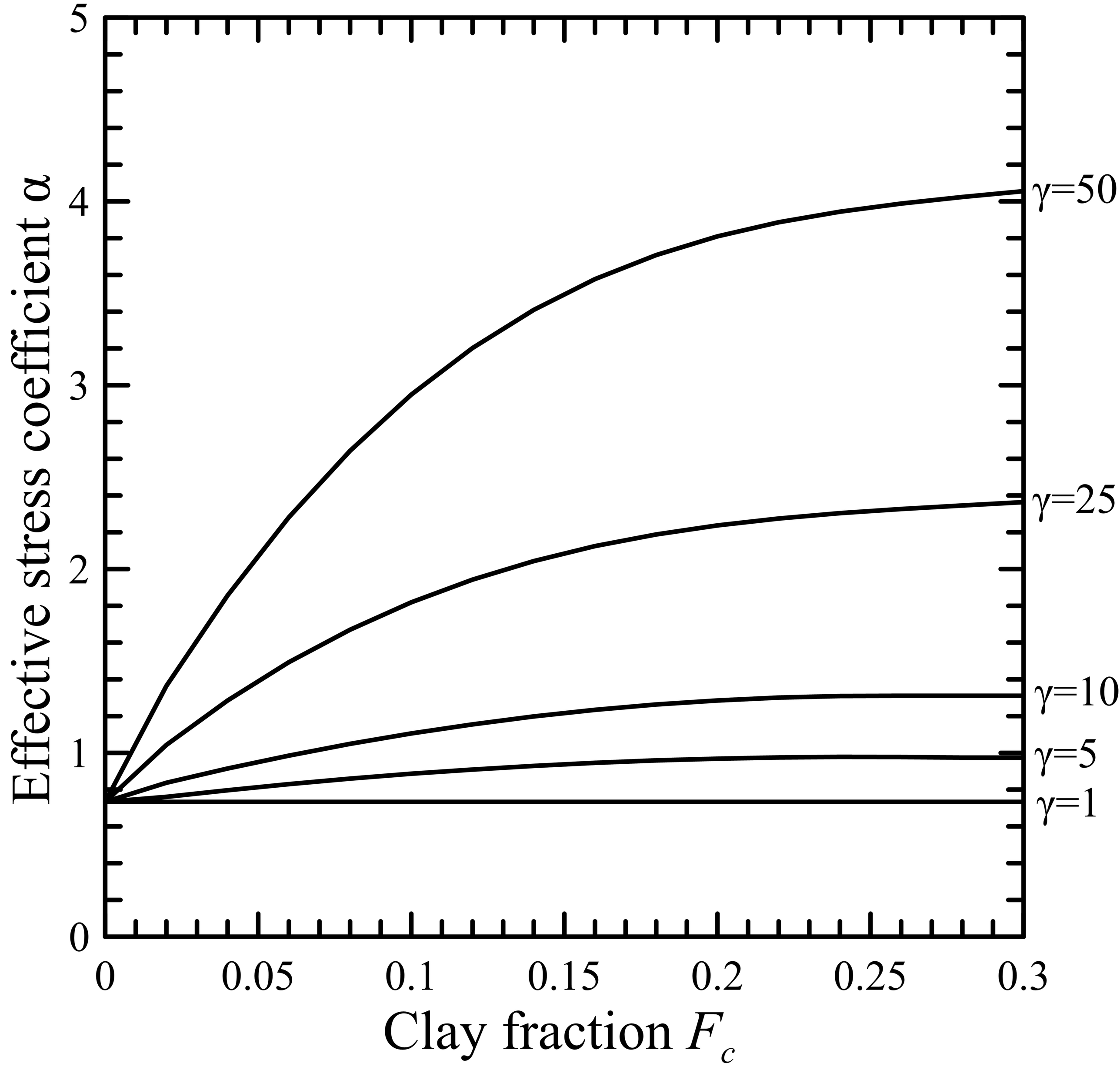
Effective stress coefficient α
Clay fraction F_c
0
1
2
3
4
5
0
0.05
0.1
0.15
0.2
0.25
0.3
γ=50
γ=25
γ=10
γ=5
γ=1

Figure 3.

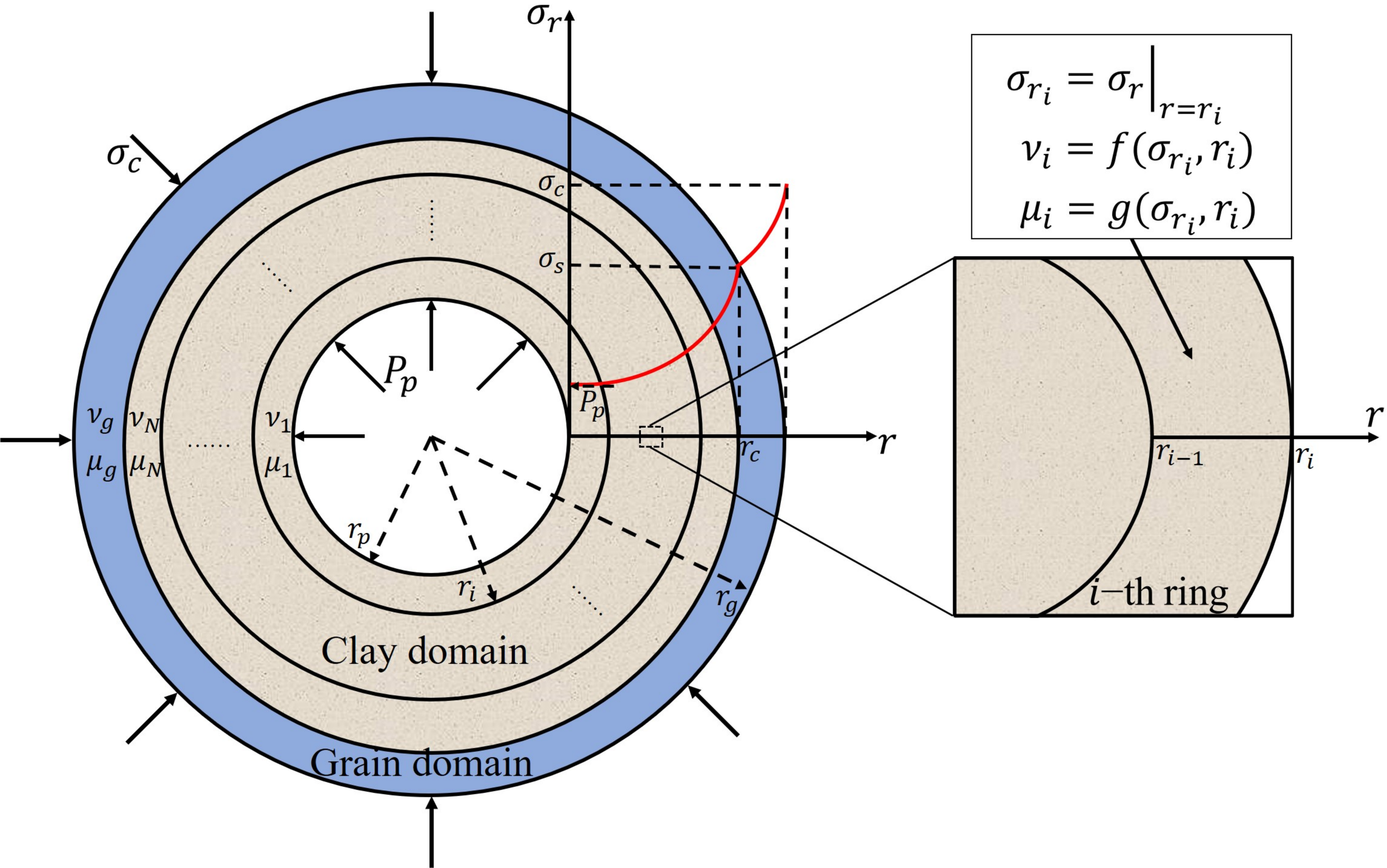
σ_r
σ_c
σ_c
σ_s
P_p
$\bar{P}_p$
ν_g
μ_g
ν_N
μ_N
ν_1
μ_1
r_p
r_i
r_c
r_g
r
Clay domain
Grain domain
$\sigma_{r_i} = \sigma_r\big|_{r=r_i}$
$\nu_i = f(\sigma_{r_i}, r_i)$
$\mu_i = g(\sigma_{r_i}, r_i)$
r_{i-1}
r_i
r
i−th ring

Figure 4.

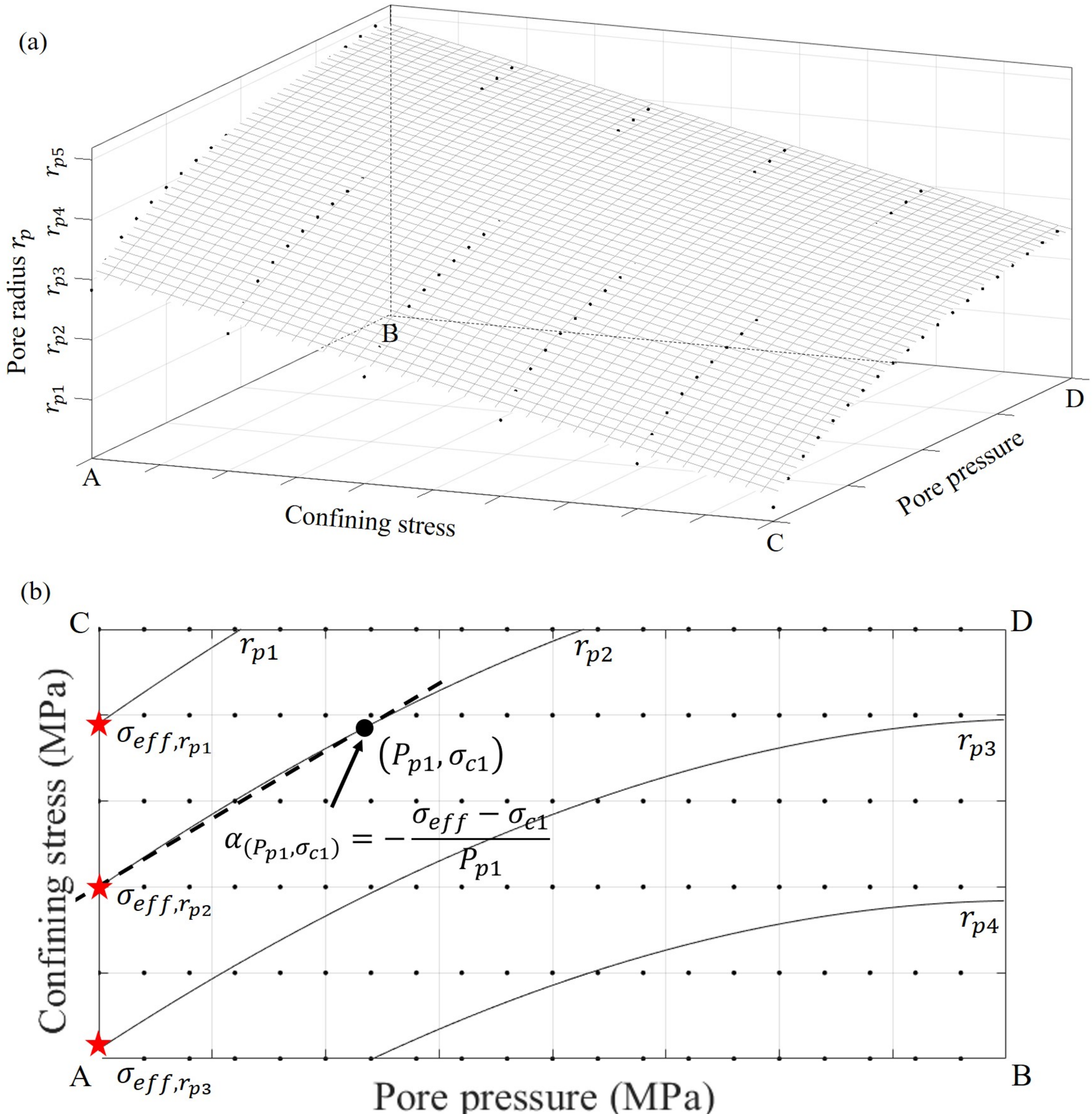
(a)
Pore radius r_p
r_{p5}
r_{p4}
r_{p3}
r_{p2}
r_{p1}
A
B
C
D
Confining stress
Pore pressure
(b)
C
D
A
B
r_{p1}
r_{p2}
r_{p3}
r_{p4}
$\sigma_{eff,r_{p1}}$
$\sigma_{eff,r_{p2}}$
$\sigma_{eff,r_{p3}}$
(P_{p1}, σ_{c1})
$\alpha_{(P_{p1},\sigma_{c1})} = -\frac{\sigma_{eff} - \sigma_{c1}}{P_{p1}}$
Confining stress (MPa)
Pore pressure (MPa)

Figure 5.

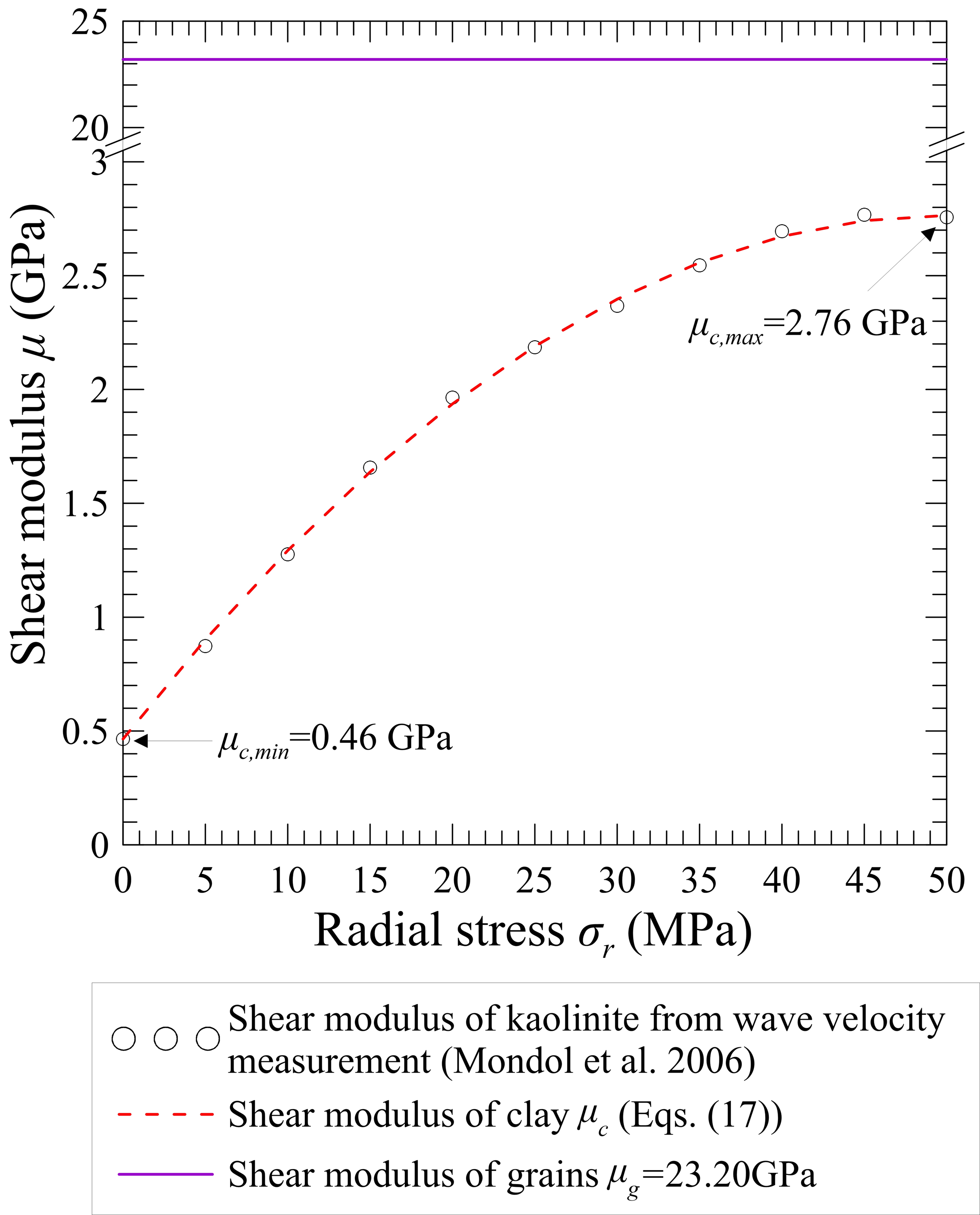
Shear modulus μ (GPa)
Radial stress σ_r (MPa)
$\mu_{c,max}$=2.76 GPa
$\mu_{c,min}$=0.46 GPa
Shear modulus of kaolinite from wave velocity measurement (Mondol et al. 2006)
Shear modulus of clay μ_c (Eqs. (17))
Shear modulus of grains μ_g=23.20GPa

Figure 6.

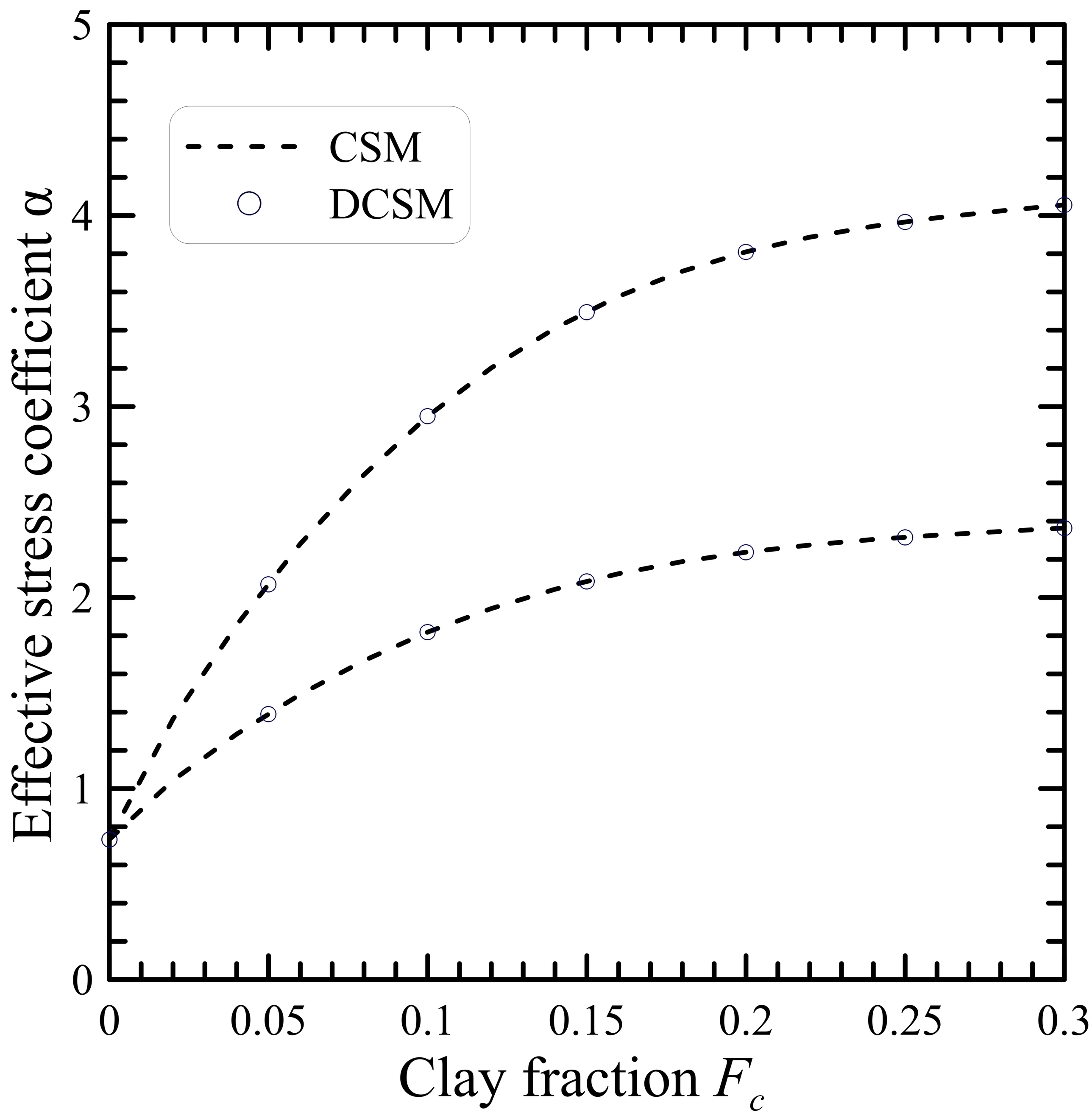
CSM
DCSM
Effective stress coefficient α
Clay fraction F_c
0
1
2
3
4
5
0
0.05
0.1
0.15
0.2
0.25
0.3

Figure 7.

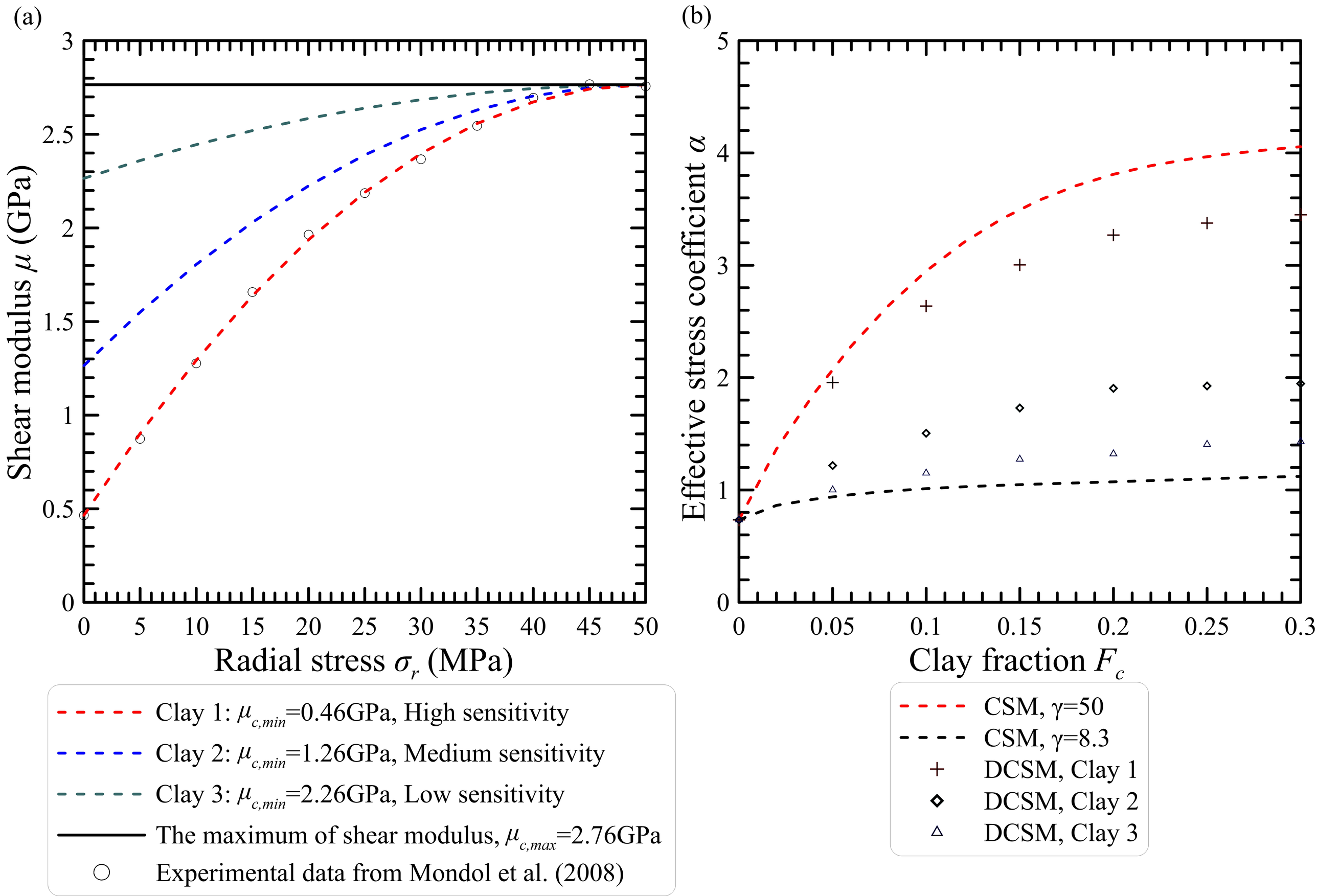
(a)
Shear modulus μ (GPa)
Radial stress σr (MPa)
0
0.5
1
1.5
2
2.5
3
0
5
10
15
20
25
30
35
40
45
50
Clay 1: μc,min=0.46GPa, High sensitivity
Clay 2: μc,min=1.26GPa, Medium sensitivity
Clay 3: μc,min=2.26GPa, Low sensitivity
The maximum of shear modulus, μc,max=2.76GPa
Experimental data from Mondol et al. (2008)
(b)
Effective stress coefficient α
Clay fraction Fc
0
1
2
3
4
5
0
0.05
0.1
0.15
0.2
0.25
0.3
CSM, γ=50
CSM, γ=8.3
DCSM, Clay 1
DCSM, Clay 2
DCSM, Clay 3

Figure 8.

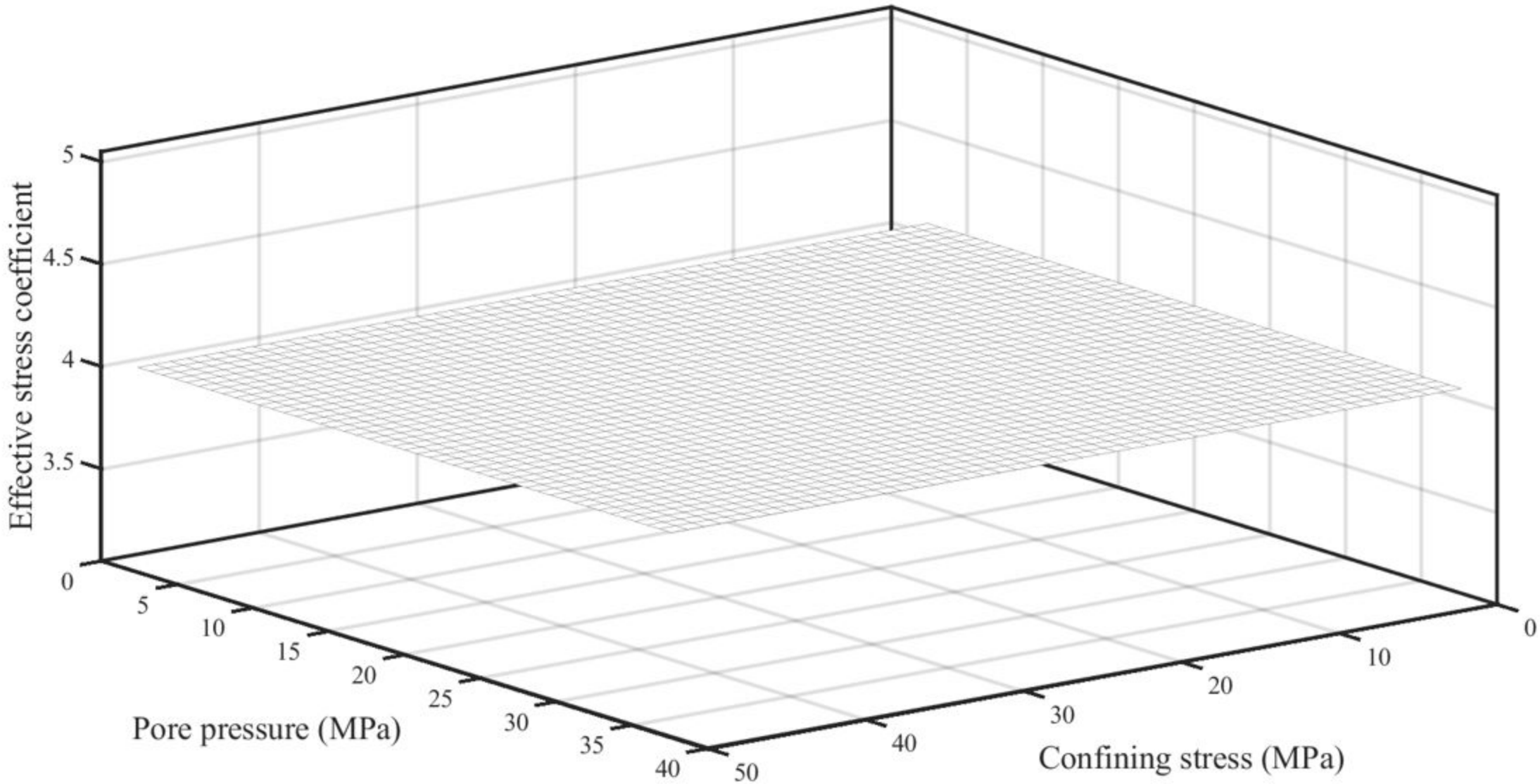
Effective stress coefficient
5
4.5
4
3.5
0
5
10
15
20
25
30
35
40
Pore pressure (MPa)
50
40
30
20
10
0
Confining stress (MPa)

Figure 9.

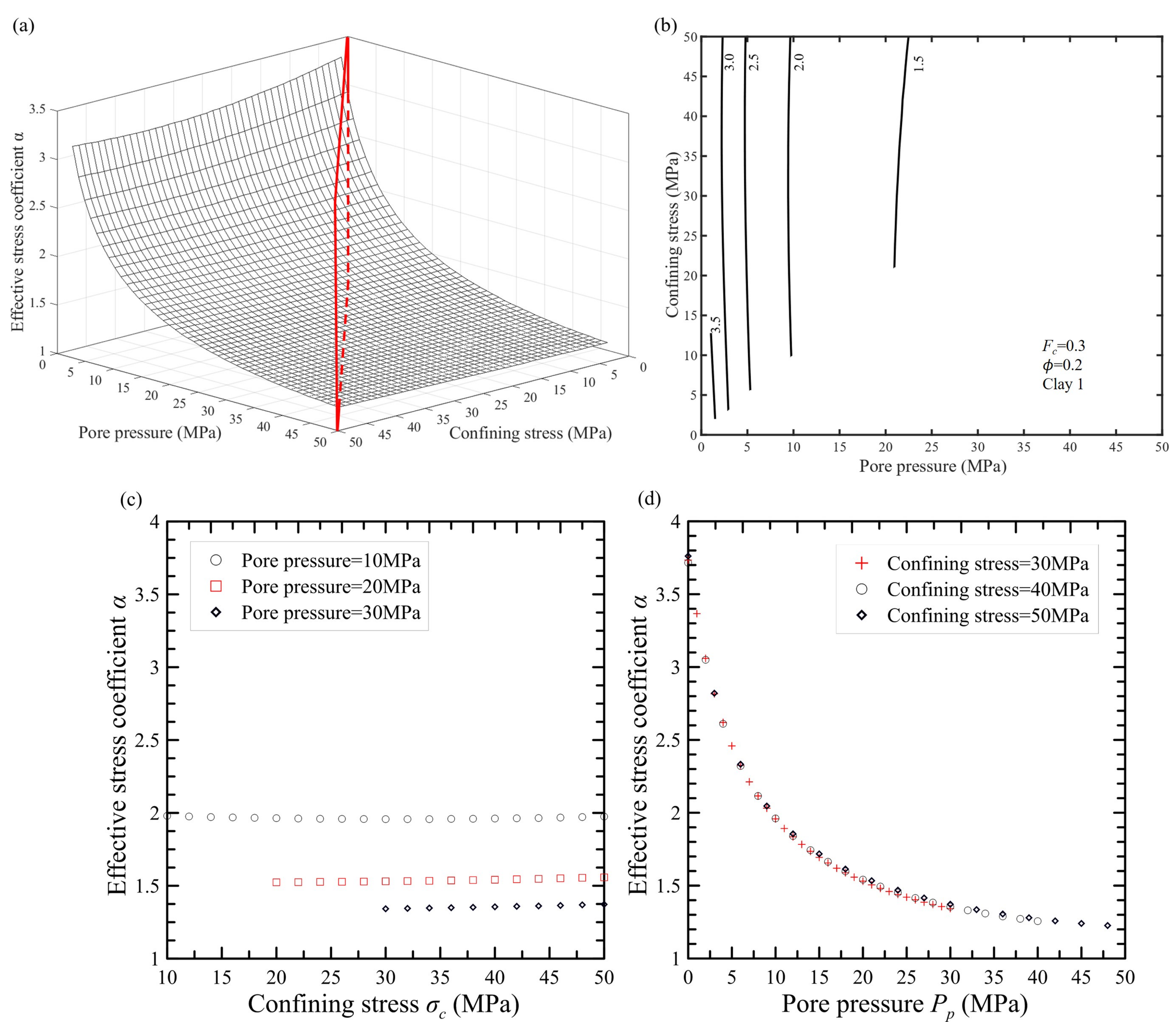
(a)
Effective stress coefficient α
Pore pressure (MPa)
Confining stress (MPa)
(b)
Confining stress (MPa)
Pore pressure (MPa)
3.5
3.0
2.5
2.0
1.5
F_c=0.3
ϕ=0.2
Clay 1
(c)
Pore pressure=10MPa
Pore pressure=20MPa
Pore pressure=30MPa
Effective stress coefficient α
Confining stress σ_c (MPa)
(d)
Confining stress=30MPa
Confining stress=40MPa
Confining stress=50MPa
Effective stress coefficient α
Pore pressure P_p (MPa)

Figure 10.

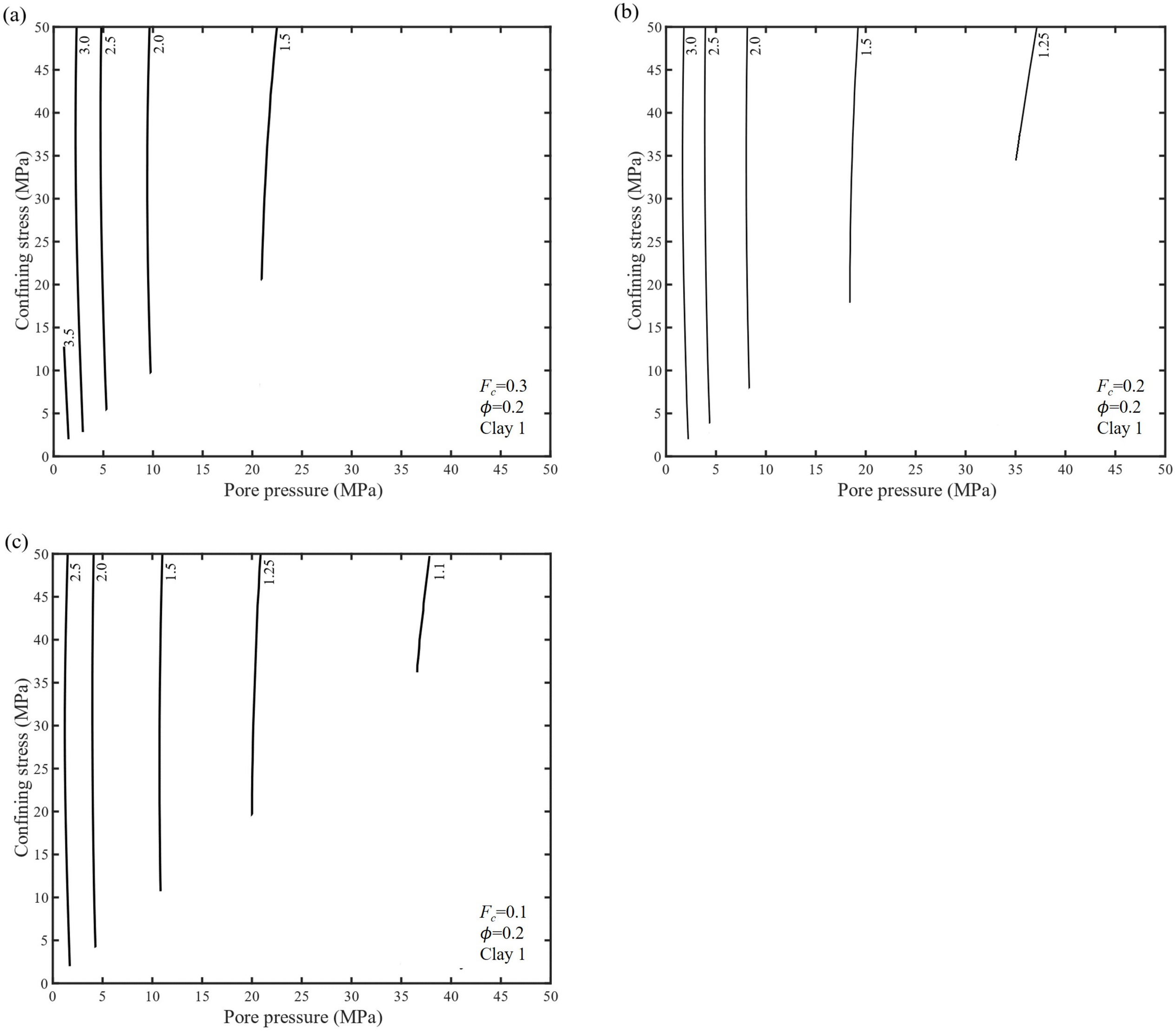
(a)
Confining stress (MPa)
Pore pressure (MPa)
3.5
3.0
2.5
2.0
1.5
F_c=0.3
ϕ=0.2
Clay 1
(b)
Confining stress (MPa)
Pore pressure (MPa)
3.0
2.5
2.0
1.5
1.25
F_c=0.2
ϕ=0.2
Clay 1
(c)
Confining stress (MPa)
Pore pressure (MPa)
2.5
2.0
1.5
1.25
1.1
F_c=0.1
ϕ=0.2
Clay 1

Figure 11.

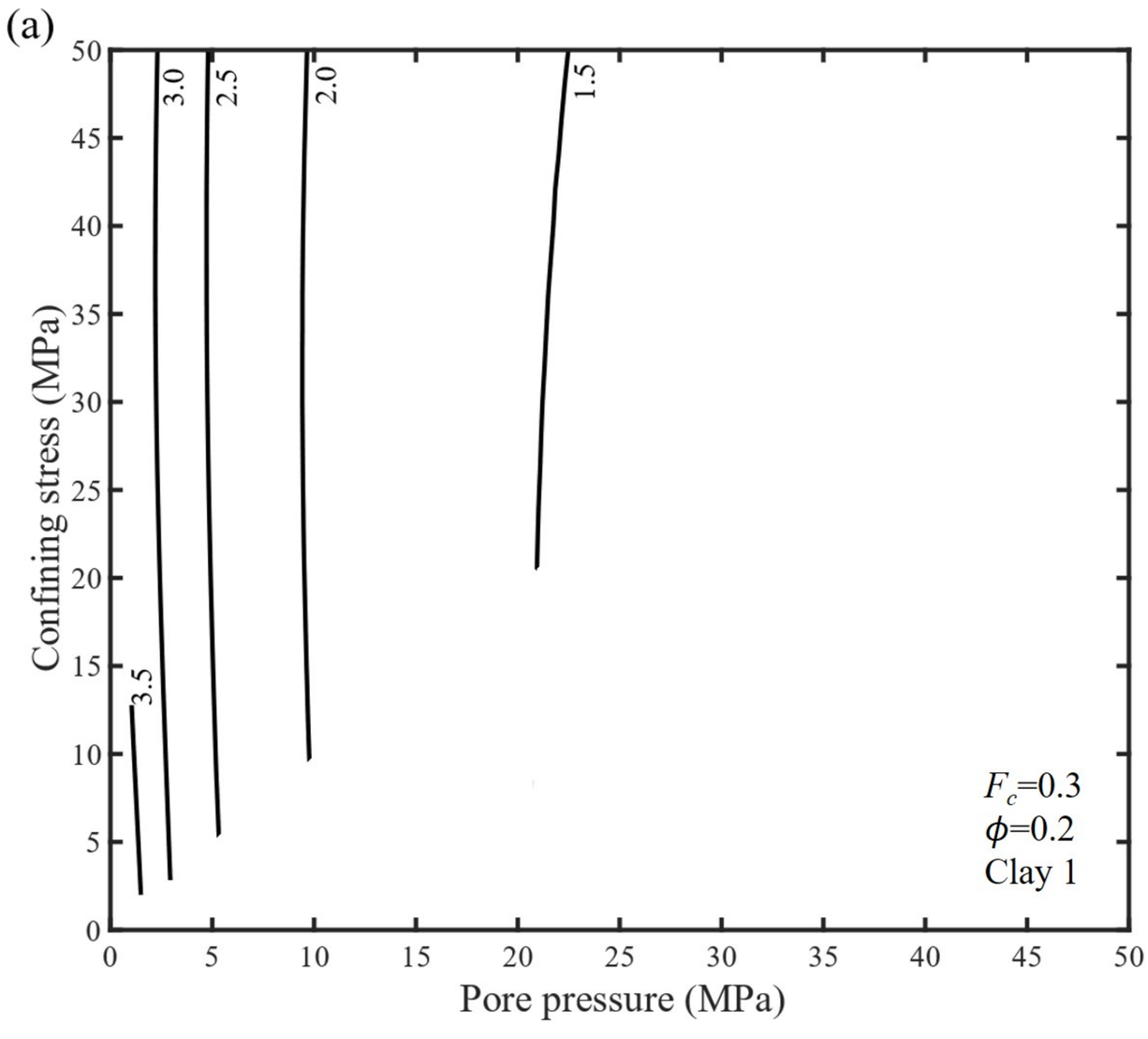
(a)
Confining stress (MPa)
Pore pressure (MPa)
3.5
3.0
2.5
2.0
1.5
F_c=0.3
ϕ=0.2
Clay 1

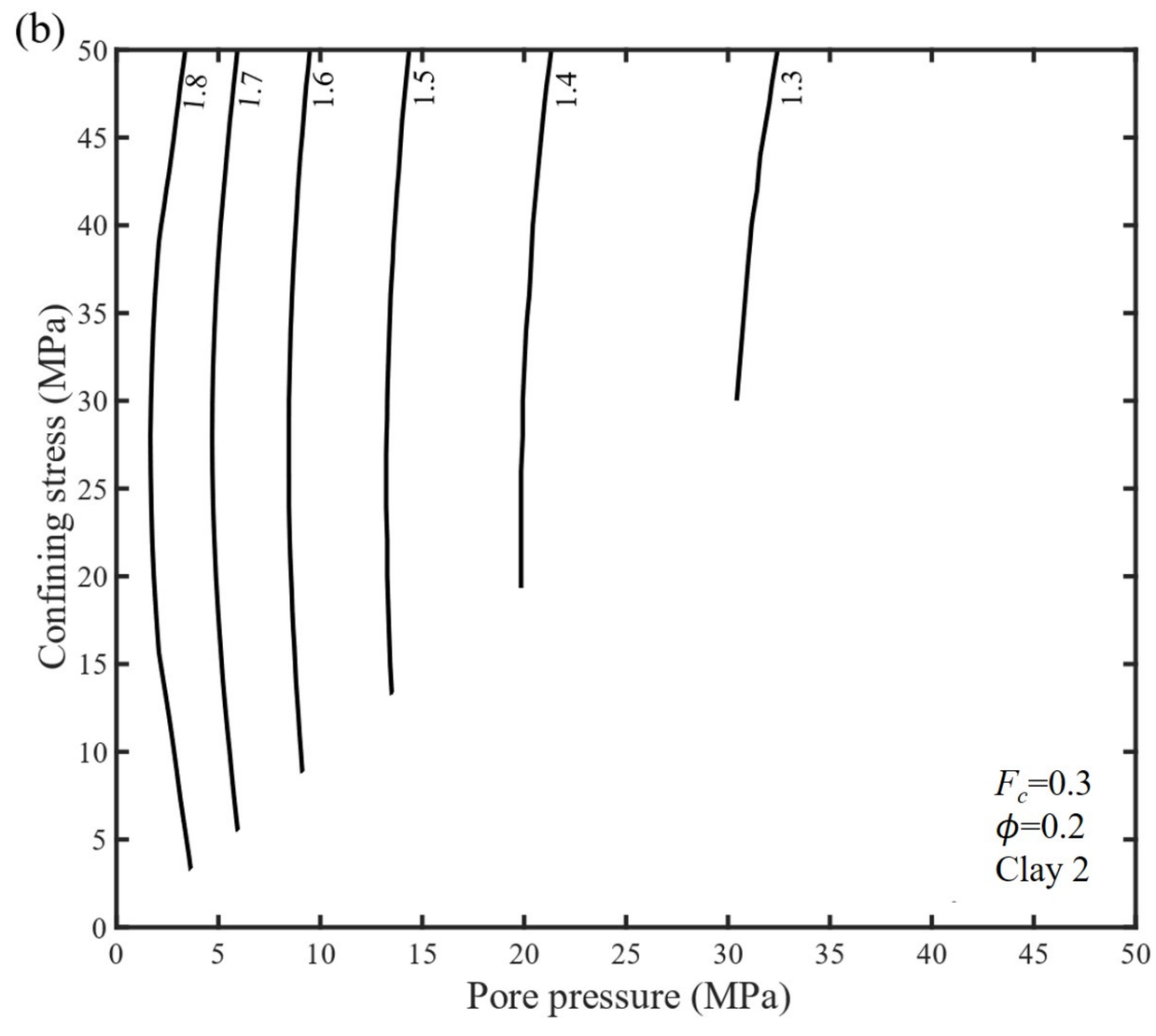
(b)
Confining stress (MPa)
Pore pressure (MPa)
1.8
1.7
1.6
1.5
1.4
1.3
F_c=0.3
ϕ=0.2
Clay 2

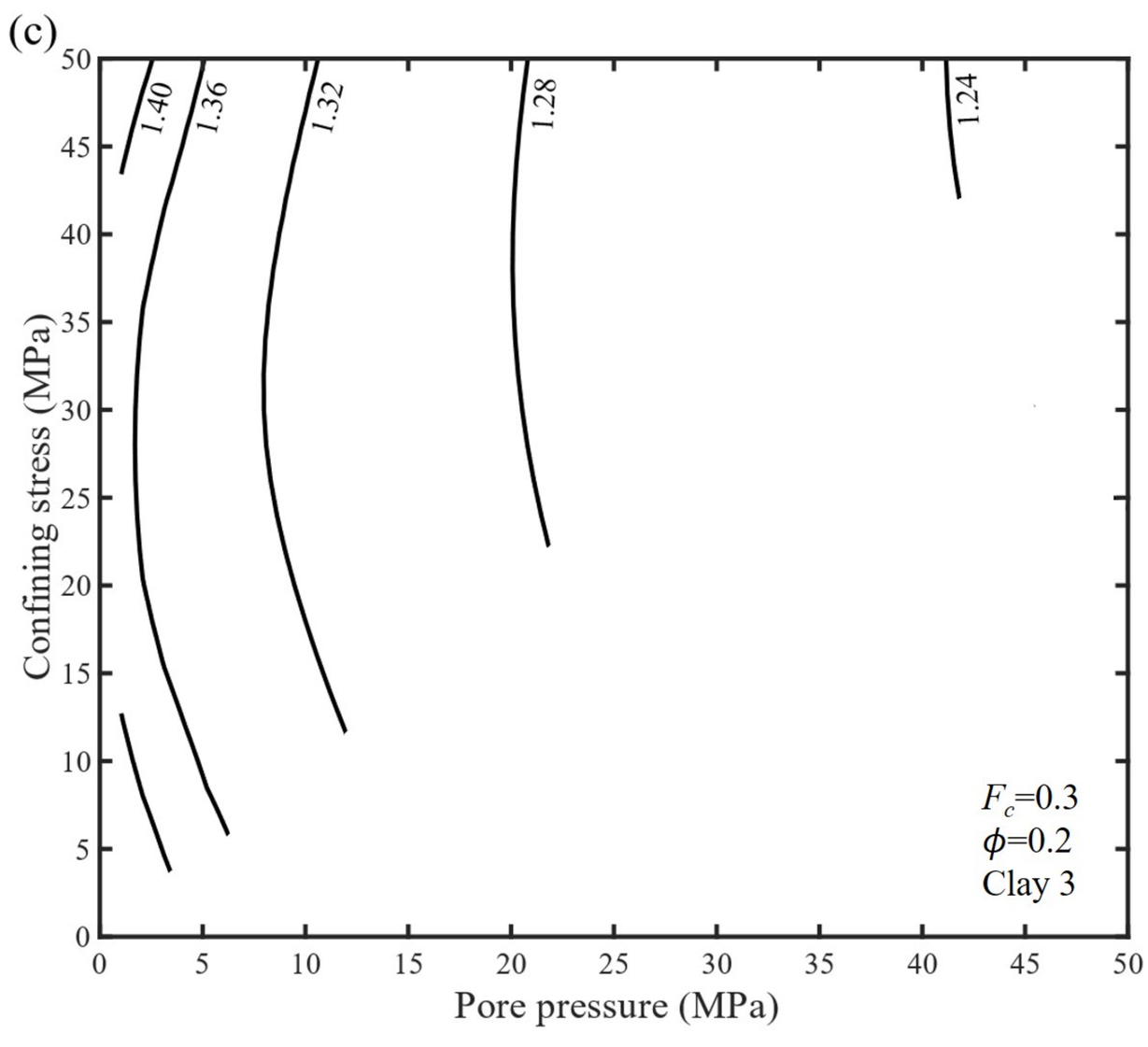
(c)
Confining stress (MPa)
Pore pressure (MPa)
1.40
1.36
1.32
1.28
1.24
F_c=0.3
ϕ=0.2
Clay 3

Figure 12.

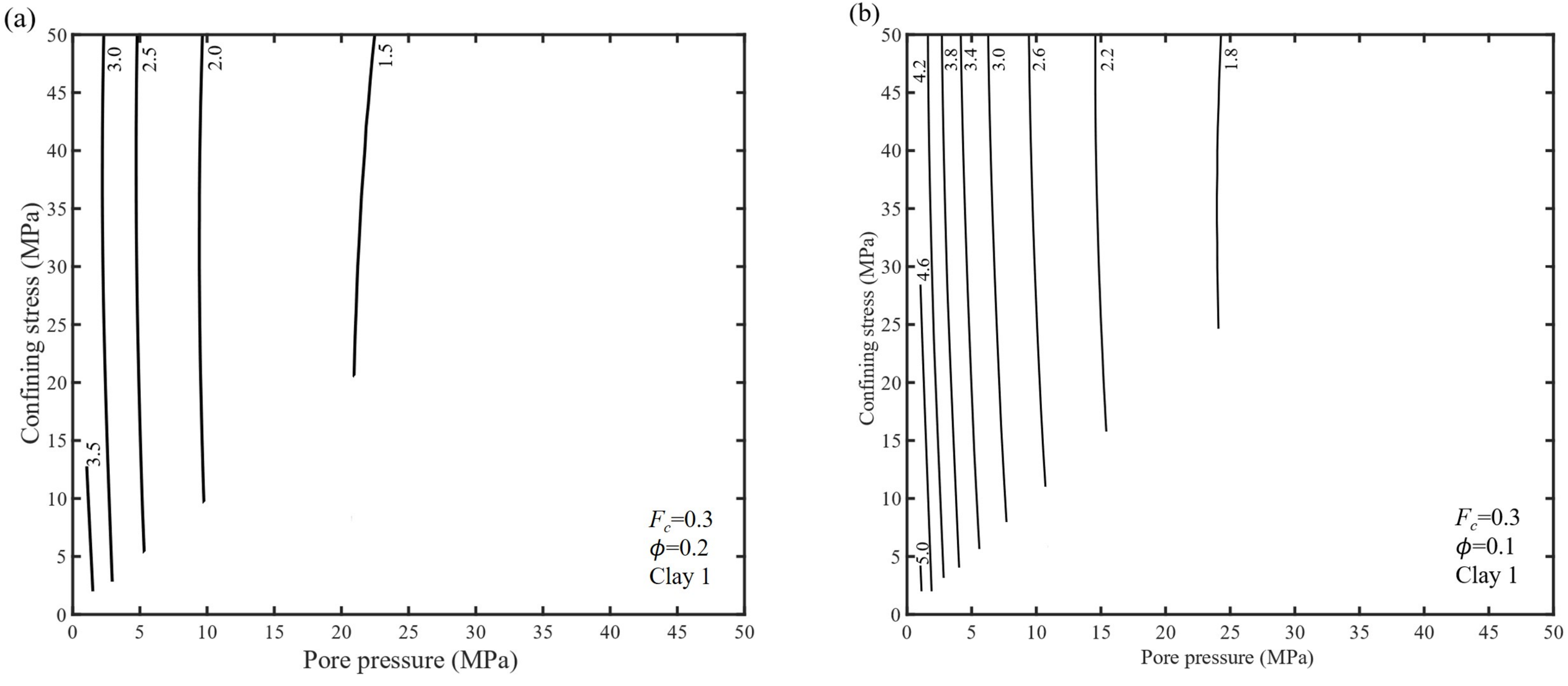
(a)
Confining stress (MPa)
Pore pressure (MPa)
3.5
3.0
2.5
2.0
1.5
F_c=0.3
ϕ=0.2
Clay 1
(b)
Confining stress (MPa)
Pore pressure (MPa)
5.0
4.6
4.2
3.8
3.4
3.0
2.6
2.2
1.8
F_c=0.3
ϕ=0.1
Clay 1

Figure 13.

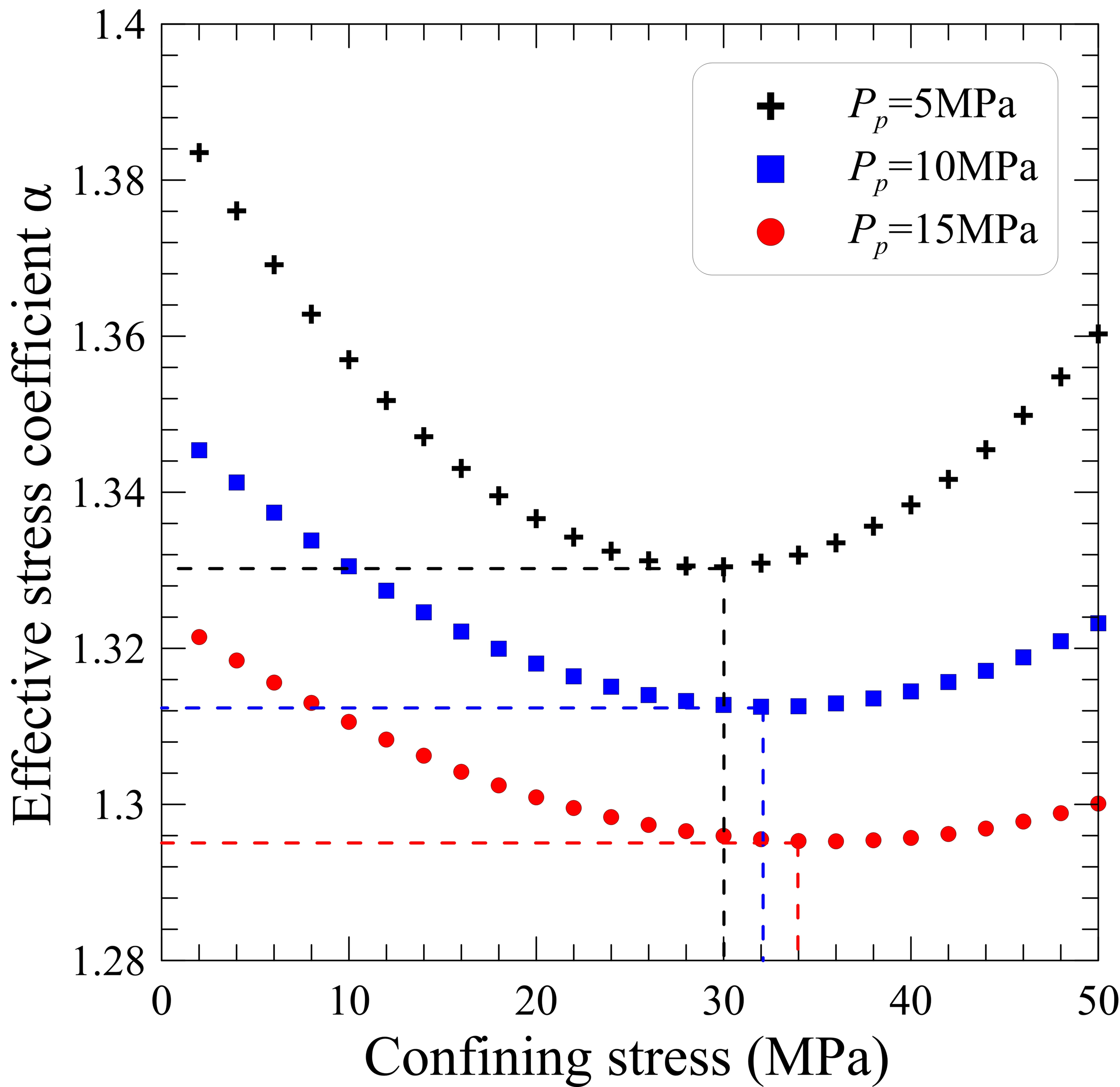
Effective stress coefficient α
Confining stress (MPa)
P_p=5MPa
P_p=10MPa
P_p=15MPa
1.4
1.38
1.36
1.34
1.32
1.3
1.28
0
10
20
30
40
50

Figure 14.

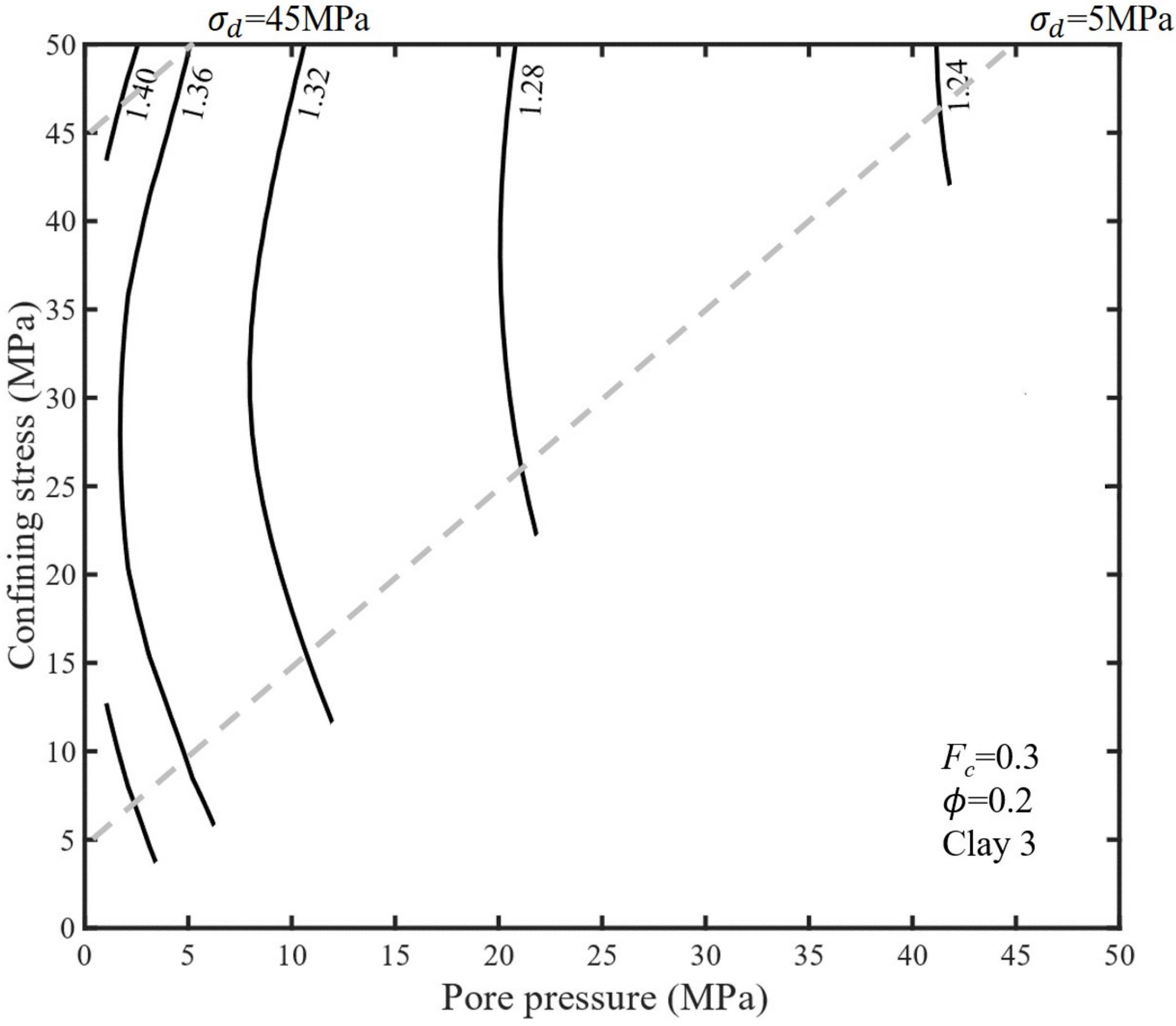
σ_d=45MPa
σ_d=5MPa
1.40
1.36
1.32
1.28
1.24
F_c=0.3
ϕ=0.2
Clay 3
Confining stress (MPa)
Pore pressure (MPa)
0
5
10
15
20
25
30
35
40
45
50

Figure 15.

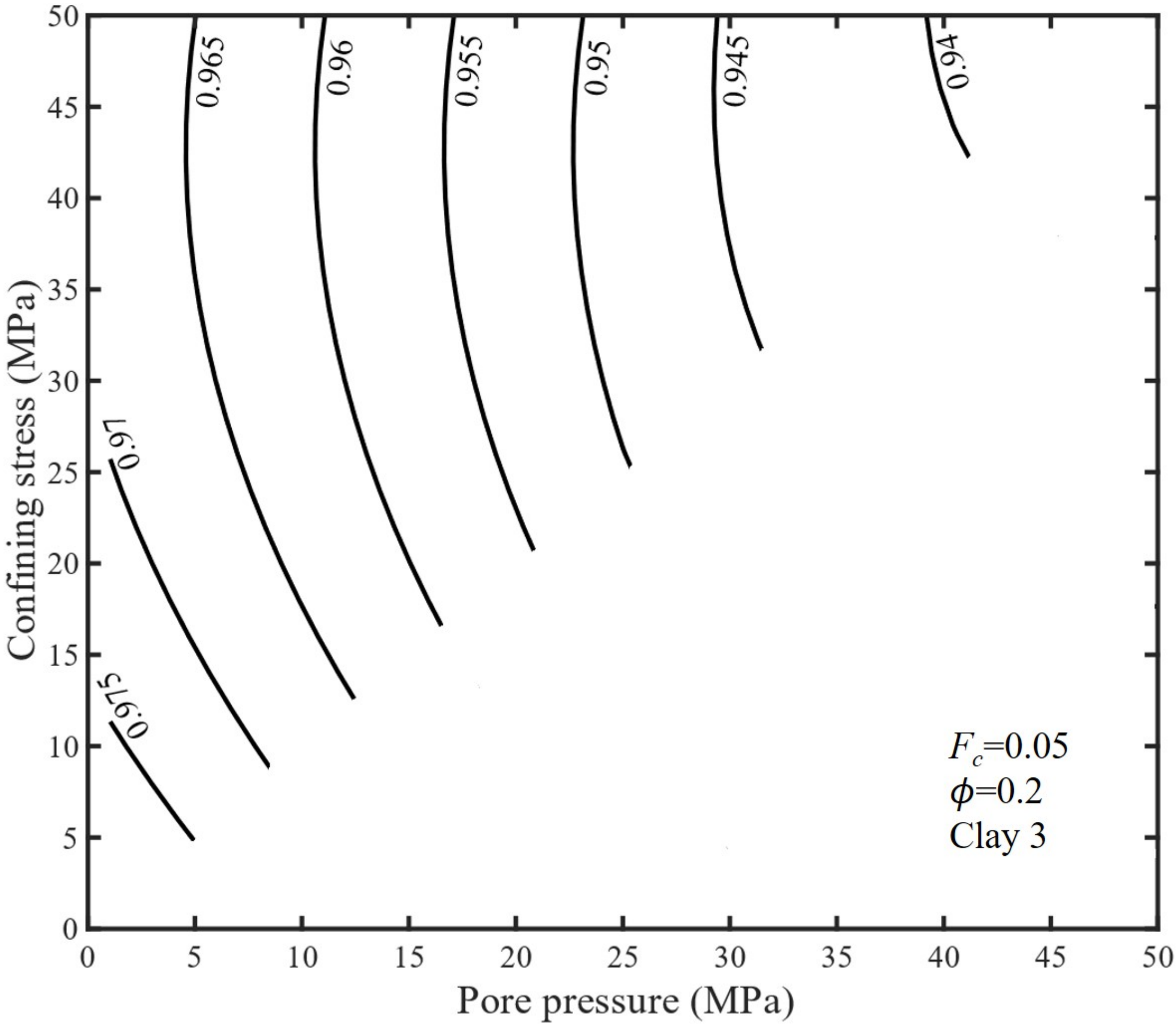
0.965
0.96
0.955
0.95
0.945
0.94
0.97
0.975
F_c=0.05
ϕ=0.2
Clay 3
Confining stress (MPa)
Pore pressure (MPa)
0
5
10
15
20
25
30
35
40
45
50

Figure 16.

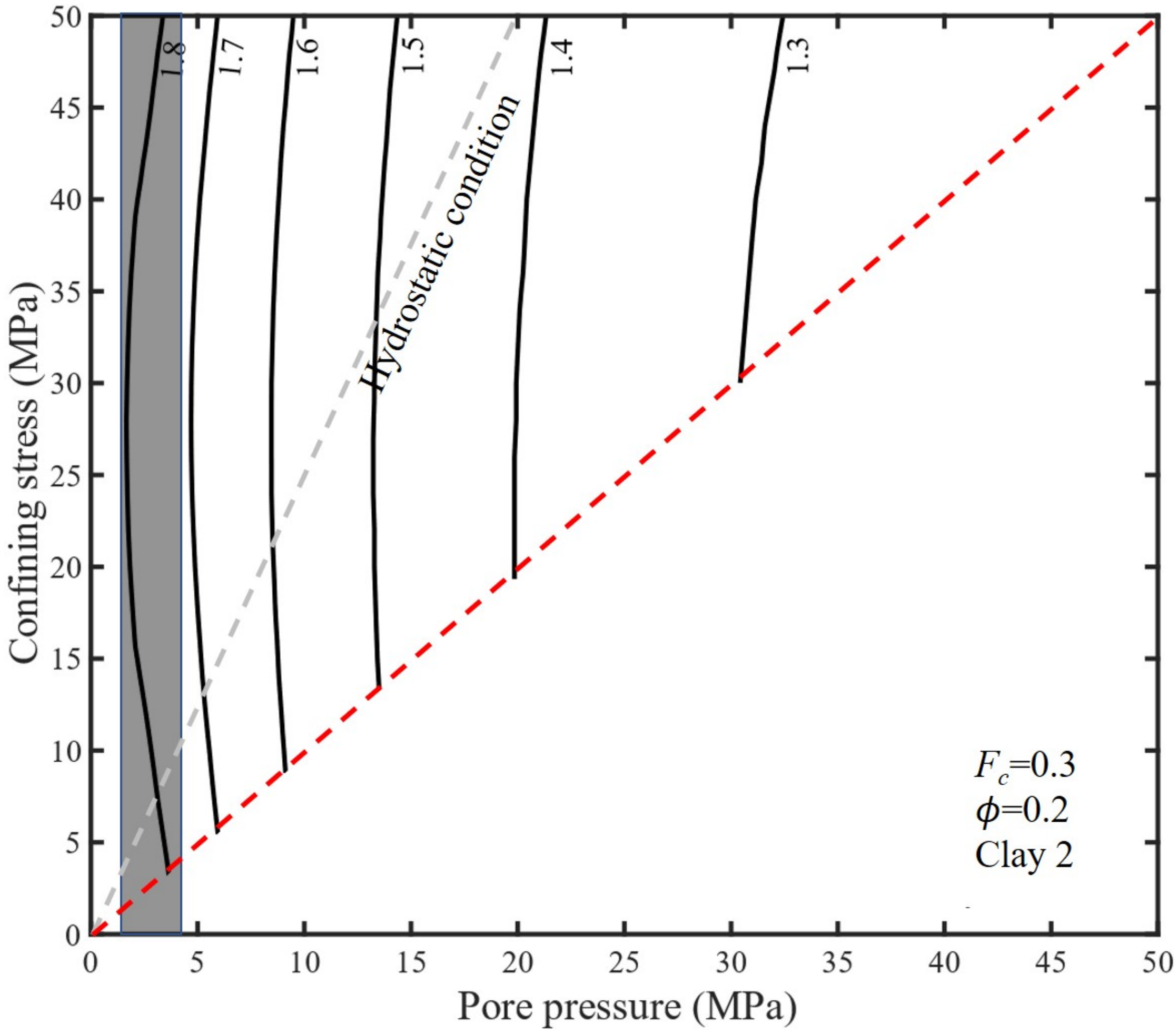
1.8
1.7
1.6
1.5
1.4
1.3
Hydrostatic condition
F_c=0.3
ϕ=0.2
Clay 2
Confining stress (MPa)
Pore pressure (MPa)
0
5
10
15
20
25
30
35
40
45
50

Figure 17.

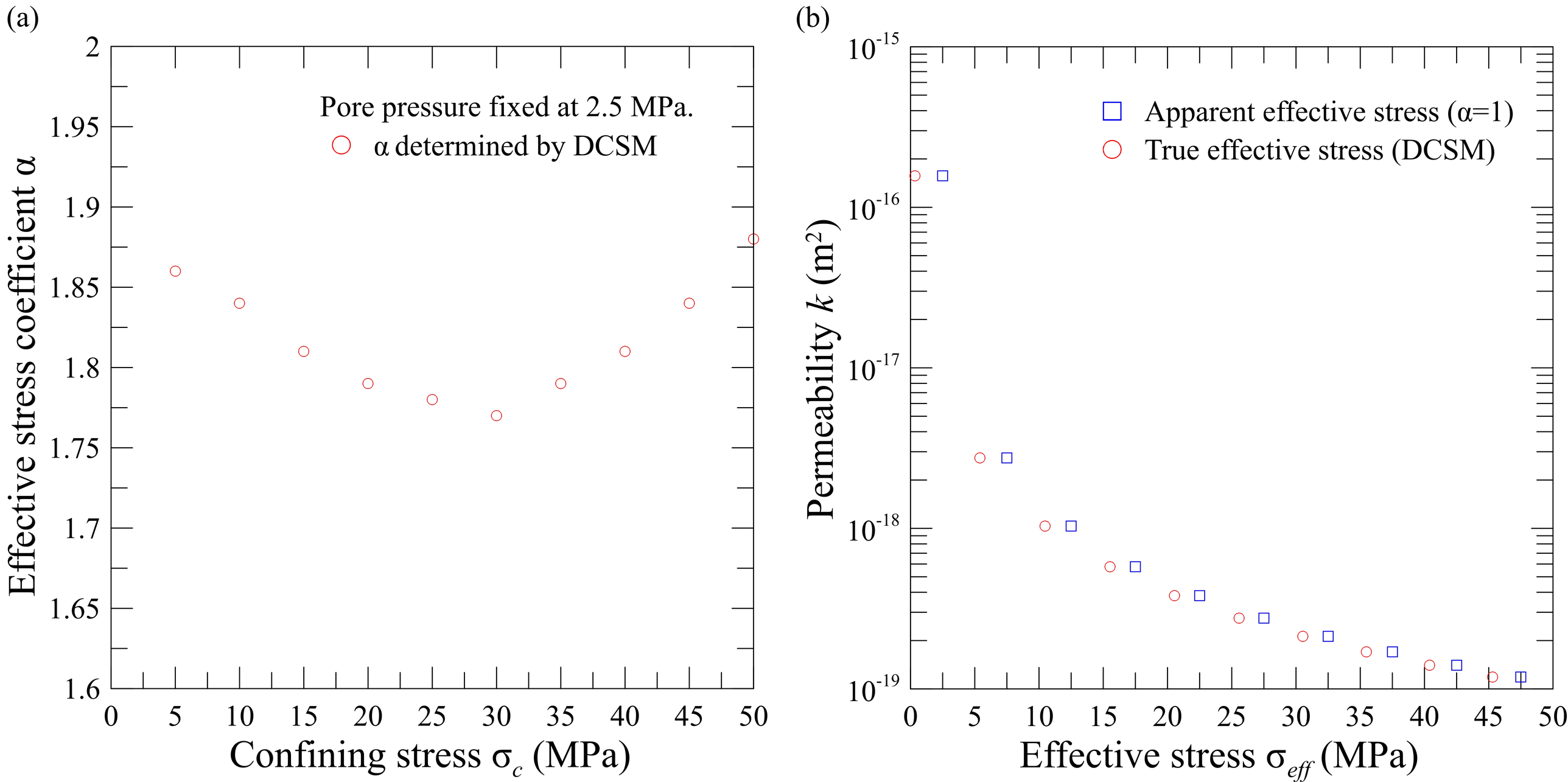
(a)
Pore pressure fixed at 2.5 MPa.
α determined by DCSM
Effective stress coefficient α
Confining stress σc (MPa)
2
1.95
1.9
1.85
1.8
1.75
1.7
1.65
1.6
0
5
10
15
20
25
30
35
40
45
50
(b)
Apparent effective stress (α=1)
True effective stress (DCSM)
Permeability k (m2)
Effective stress σeff (MPa)
10-15
10-16
10-17
10-18
10-19

Figure 18.

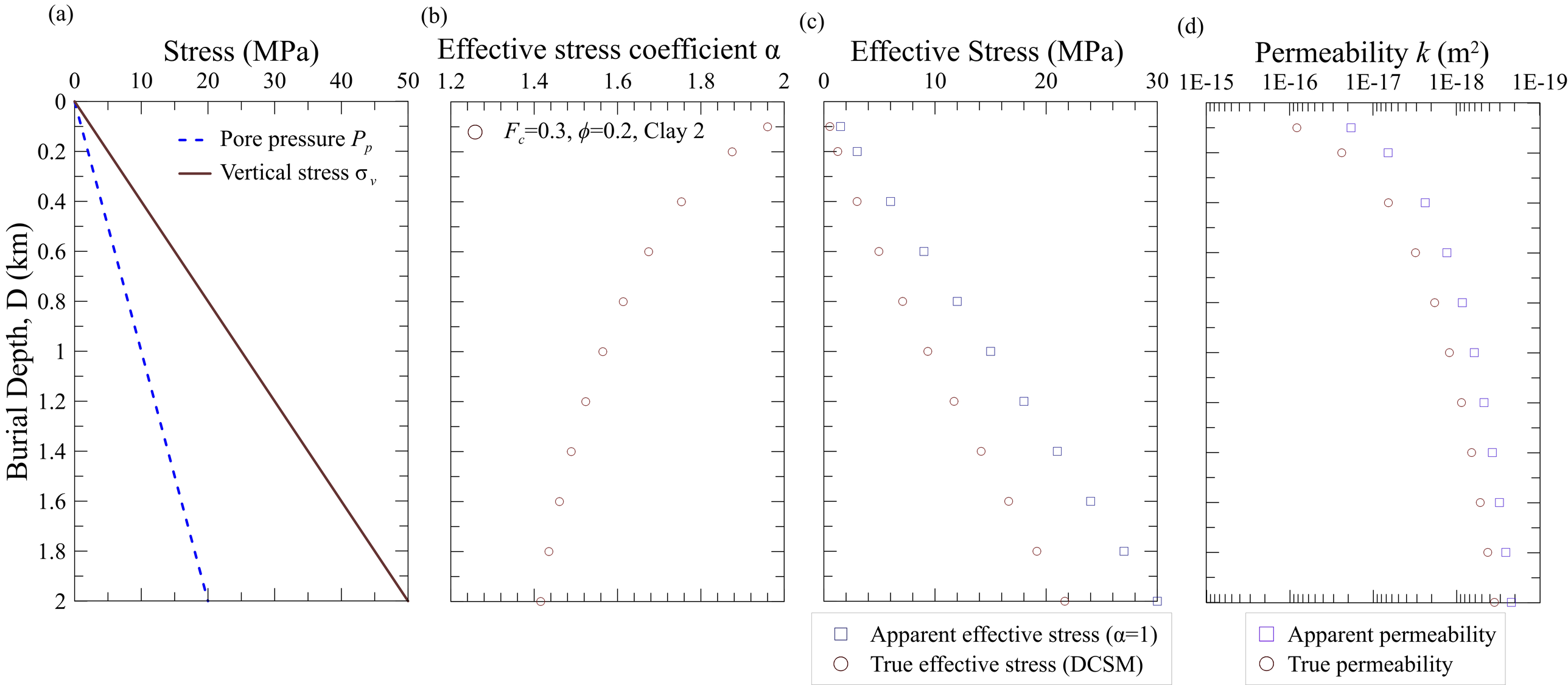
(a)
Stress (MPa)
0
10
20
30
40
50
Burial Depth, D (km)
0
0.2
0.4
0.6
0.8
1
1.2
1.4
1.6
1.8
2
Pore pressure P_p
Vertical stress σ_v
(b)
Effective stress coefficient α
1.2
1.4
1.6
1.8
2
F_c=0.3, ϕ=0.2, Clay 2
(c)
Effective Stress (MPa)
0
10
20
30
Apparent effective stress (α=1)
True effective stress (DCSM)
(d)
Permeability k (m^2)
1E-15
1E-16
1E-17
1E-18
1E-19
Apparent permeability
True permeability